SIMPLE FINITE ELEMENTS FOR NONLINEAR
ANALYSIS OF FRAMED STRUCTURES

Reijo KOUHIA

SUMMARY: In this study a finite element method for both geometrically and materially nonlinear analyses of space frames is developed. Beams with both solid and thin-walled open cross-sections have been considered. The equations of equilibrium have been formulated using an updated incremental Lagrangian description. The elements developed can undergo large displacements and rotations, but the incremental rotations are assumed to be small. The material models adopted are elasto-plastic, temperature dependent elasto-plastic and visco-plastic models with special reference to metals. Also computationally more economical formulations based on the relationship between stress resultants and generalized strain quantities have been presented. In the case of thin-walled beams the torsional behaviour is modelled using a two parametric deplanation model, where the angle of twist and it's derivative have independent approximations. This approach yields the average warping shear strains directly from the displacement assumptions and no discrepancy between stress and strain fields exists.

INTRODUCTION

Frames are common load carrying systems in engineering constructions. Effective use of high strength materials and the tendency to optimazed constructions result in thin and slender structures. Due to the slenderness and increased imperfection sensitivity the stability problems become more significant. The character of the load deformation path in the post-buckling range is important in assessing the safety of the structure. Coupled geometrical and material nonlinearities complicate the structural analysis, and only numerical solutions are feasible in practical cases.

The earliest numerical analysing procedures for the nonlinear response of space frames were mainly based on the beam-column theory, where the effect of axial forces to the behaviour of the frame is taken into account, e.g. Renton (1962), Connor et al. (1968), Chu and Rampetsreiter (1973), Papandrakakis (1981) and Virtanen and Mikkola (1985). In those approaches the tangent stiffness matrix is formulated using the exact solution of the differential equation for a beam-column. It gives good accuracy in cases

3

where the moments of inertia in the principal directions of the cross section are of same magnitude. In cases where the axial forces are small or the cross-section moments of inertia differ greatly, i.e. in lateral buckling problems, the analyses of space structures with the beam-column elements do not give satisfactory results.

The noncommutative nature of finite rotations in three dimensional space complicates the formulation of incremental equilibrium equations, capable for handling large rotation increments. Several studies for handling the large rotation effects can be found in References, e.g. Argyris et al. (1978), Argyris (1982), Simo (1985), Cardona and Geradin (1988), Dvorkin et al. (1988), Friberg (1988a, b). Argyris et al. (1978) have introduced the semitangential rotation concept. In contrast to rotation about fixed axes these semitangential rotations which correspond to the semitangential torque of Ziegler (1968) possess the most important property of being commutative. Simo and Vu-Quoc (1986) have developed the configuration update procedure which is the algorithmic counterpart of the exponential map and the computational implementation relies on the formula for the exponential of a skew-symmetric matrix. In this Eulerian approach the tangent operator is non-symmetric in non-equilibrium configuration but the symmetry is shown to be recovered at equilibrium provided that the loading is conservative. Cardona and Geradin (1988) have used the rotational vector to parametrize rotations. They have treated Eulerian, total- and updated Lagrangian formulations. As pointed out by Cardona and Geradin (1988) an Eulerian approach allows, on one hand, a relatively simple derivation of fully linearized operators but, on the other hand these opeators are non-symmetric in a general case. Full symmetry of operators is obtained in the Lagrangian approach. Large deflection finite element formulations have been presented by e.g. Belytschko et al. (1977), Bathe and Bolourchi (1979), Remseth (1979). In these studies the nonlinear equations of motion have been formulated by the total Lagrangian or by the updated Lagrangian approach. In large deflection problems of beams the updated formulation has been found to be more economical and convenient than the total Lagrangian formulation, Bathe and Bolourchi (1979). A total Lagrangian formulation does not allow an easy manipulation of rotations exceeding the value of π, Cardona and Geradin (1988). Recently Sandhu et al. (1990) have used a co-rotational formulation in deriving the equations of equilibrium for a curved and twisted beam element. In the co-rotational formulation the rigid body motion is eliminated from the total displacements.

In all of the above mentioned studies the warping torsion has not been taken into account. The stiffness matrix of a thin-walled beam seems to have been first presented by Krahula (1967). The effects of initial bending moments and axial forces have been considered by Krajcinovic (1969), Barsoum and Gallagher (1970), Friberg (1985) and many others. Mottershead (1988a,b) has extended the semiloof beam element to include warping torsion of beams with thin-walled open cross-section. All the above mentioned studies have considered linear stability problems. The effect of pre-buckling deflections to the critical loads have been studied by, e.g. Attard (1986) and van Erp

4

(1989). Computational tools for nonlinear post-buckling analyses have been presented by Rajasekaran and Murray (1973), Besseling (1977), Hasegawa et al. (1987a,b), van Erp et al. (1988). Bažant and El Nimeiri (1973) have formulated the finite element equilibrium equations of a thin-walled beam element for large deflection analysis, taking into account also initial bimoments. The study of Rajasekaran and Murray (1973) includes also elasto-plastic material properties. The above mentioned studies for thin-walled beams have utilized the Vlasov's theory of torsion and the Euler-Bernoulli theory for bending of thin beams. Seculović (1986) has proposed an alternative formulation which takes into account also the shear deformation in the middle line of the cross-section. In this formulation the warping of the cross-section is described by a set of axial displacement parameters, the number of which depends on the shape of the cross-section. It is also applicable for both closed and open cross-sections. Both Epstein and Murray (1976) and Chen and Blandford (1989) have suggested a formulation which takes into account the average shear strains due to warping torsion. Chen and Blandford presented a C^0 beam element for linear analysis while Epstein and Murray formulated an element capable for nonlinear problems.

Wunderlich et al. (1986) have used an incremental updated Lagrangian description in the derivation of the basic beam equations from a generalized variational principle. They have explored the influence of loading configuration, material parameters, geometric nonlinearities and warping constraints on the load-carrying behaviour and on the bifurcation and ultimate loads of thin-walled beam structures. The influence of material parameters have been investigated with both J_2 flow and deformation theories of plasticity. In their study the tangential stiffness matrices are obtained by direct numerical integration of the governing incremental differential equations and no a priori assumptions on the distribution of the field quantities have been made as in conventional finite element analyses.

A nonlinear theory of elastic beams with thin-walled open cross-sections has been derived by Møllmann (1981). In this theory the beam is regarded as a thin shell, and the appropriate geometrical constraints are introduced which constitute a generalization of those employed in Vlasov's linear theory. The rotations of the beam are described by means of a finite rotation vector. Computational results based on this theory have been presented by Pedersen (1982a,b) in which Koiter's general theory of elastic stability is used to carry out a perturbation analysis of the buckling and post buckling behaviour.

EQUATIONS OF EQUILIBRIUM

The sum of internal and external virtual works has to be zero for a body in an equilibrium state. Expressed in terms of Eulerian quantities the equation of virtual work has the form

$$\int_v \mathbf{T} : \delta \mathbf{D} dt dv = \int_{\partial v} \bar{\mathbf{t}}_n \cdot \delta \mathbf{u} ds + \int_v \rho(\bar{\mathbf{f}} - \ddot{\mathbf{x}}) \cdot \delta \mathbf{u} dv, \qquad (1)$$

where δ means the variation and $\mathbf{D}$ is the rate of deformation tensor, i.e. the symmetric part of the velocity gradient tensor $\mathbf{L} = \text{grad}\dot{\mathbf{x}}$, $\mathbf{T}$ the Cauchy stress tensor, $\bar{\mathbf{t}}_n, \bar{\mathbf{f}}$

5

the traction and body force vectors, $\mathbf{u}$ the displacement vector, $\mathbf{x}$ the material point coordinate vector and ρ the material density. The superimposed dots denote the time derivative. Equation (1) can be formulated in the reference configuration using the second Piola-Kirchhoff stress $\mathbf{S}$ and the corresponding deformation measure, the Green-Lagrange strain tensor $\mathbf{E} = (\mathbf{F}^T \cdot \mathbf{F} - \mathbf{I})/2$ ($\mathbf{F}$ the deformation gradient tensor), i.e.

$$\int_V \mathbf{S} : \delta \mathbf{E} \, dV = \int_{\partial V} \bar{\mathbf{t}}_N \cdot \delta \mathbf{u} \, dS + \int_V \rho_o(\bar{\mathbf{f}} - \ddot{\mathbf{x}}) \cdot \delta \mathbf{u} \, dV, \tag{2}$$

in which $\mathbf{H} = \mathbf{F} - \mathbf{I}$ is the displacement gradient, $\bar{\mathbf{t}}_N$ the traction vector per unit reference area

$$\bar{\mathbf{t}}_N dS = J\mathbf{T} \cdot \mathbf{F}^{-T} \cdot \hat{\mathbf{N}} dS = \mathbf{T} \cdot \hat{\mathbf{n}} ds = \bar{\mathbf{t}}_n ds,$$

where $J = \det \mathbf{F}$. The virtual work expression (2) is used as a basis in the numerical computations.

Solution of the nonlinear equation (2) is obtained step by step and therefore it's incremental form is required. It is now assumed, that the solution has achieved configuration C_1, and the solution for an adjacent configuration C_2 is looked for. The incremental decompositions of stress and strain are

$$\begin{aligned} {}^2\mathbf{S} &= {}^1\mathbf{S} + \Delta\mathbf{S}, \\ {}^2\mathbf{E} &= {}^1\mathbf{E} + \Delta\mathbf{E}, \end{aligned} \tag{3}$$

and the variation of the Green-Lagrange strain at configuration C_2 is

$$\begin{aligned} \delta({}^2\mathbf{E}) &= \frac{1}{2}({}^2\mathbf{F}^T \cdot \delta\mathbf{F} + \delta\mathbf{F}^T \cdot {}^2\mathbf{F}), \\ &= \delta({}^1\mathbf{E}) + \frac{1}{2}(\Delta\mathbf{H}^T \cdot \delta\mathbf{H} + \delta\mathbf{H}^T \cdot \Delta\mathbf{H}). \end{aligned} \tag{4}$$

Substituting equations (4) and (3) into the virtual work expression (2) yields

$$\begin{aligned} &\int_V [\Delta\mathbf{S} : \delta({}^2\mathbf{E}) + (\Delta\mathbf{H} \cdot {}^1\mathbf{S}) : \delta\mathbf{H}] dV = \\ &\int_S {}^2\bar{\mathbf{t}}_N \cdot \delta\mathbf{u} \, dS + \int_V \rho_o({}^2\bar{\mathbf{f}} - \ddot{\mathbf{x}}) \cdot \delta\mathbf{u} \, dV - \int_V {}^1\mathbf{S} : \delta({}^1\mathbf{E}) dV. \end{aligned} \tag{5}$$

Two commonly used alternatives for the reference configuration are the undeformed state C_o or the last known equilibrium configuration C_1. These incremental strategies are known as total and updated Lagrangian formulations, respectively.

In the finite element method the displacement field $\mathbf{u}$ is approximated using shape functions $\mathbf{N}$ and nodal point displacement variables $\mathbf{q}$

$$\mathbf{u} = \mathbf{N}\mathbf{q}. \tag{6}$$

Substituting the approximation (6) into the virtual work equation, and expressing the stress increment in the form

$$\Delta\mathbf{S} = \mathbf{C} : \Delta\mathbf{E}, \tag{7}$$

6

where $\mathbf{C}$ is a fourth order tensor containing material parameters, yield the discretized incremental equations of motion, linearized with respect to $\Delta\mathbf{q}$

$$^1(\mathbf{K}_1 + \mathbf{K}_G)\Delta\mathbf{q} = {}^2\mathbf{Q} - \mathbf{M}^2\ddot{\mathbf{q}} - {}^1\mathbf{R}, \tag{8}$$

where $\mathbf{K}_G$ is the initial stress or geometric stiffness matrix, $\mathbf{Q}$ the external load vector, $\mathbf{R}$ the internal force vector, $\mathbf{M}$ the consistent mass matrix and $\Delta\mathbf{q}$ the incremental nodal point displacement vector. In the total Lagrangian formulation matrix $\mathbf{K}_1$ contains the linear stiffness and initial rotation matrices. In the updated Lagrangian formulation matrix $\mathbf{K}_1$ is dependent on the incremental displacement between configurations C_1 and C_2.

If the surface tractions depend on displacement configuration, an additional difficulty is encountered. It is assumed that the surface traction vector can be expressed as a function of a single parameter λ, i.e.

$$^2\bar{\mathbf{t}} = {}^2\lambda^2\bar{\mathbf{t}}_r, \qquad {}^2\bar{\mathbf{t}}_r = \bar{\mathbf{t}}_r({}^2\mathbf{u}), \tag{9}$$

where $\bar{\mathbf{t}}_r$ is a reference traction vector, dependent on the deformations. However, the displacements $^2\mathbf{u}$ are unknown quantities and the traction vector $^2\bar{\mathbf{t}}$ has to be approximated by the equation

$$^2\bar{\mathbf{t}} \approx {}^2\lambda^1\bar{\mathbf{t}}_r + \frac{\partial^1\bar{\mathbf{t}}}{\partial\mathbf{u}}\Delta\mathbf{u}. \tag{10}$$

For further details on displacement dependent loadings see Hibbit (1979), Argyris et al. (1982), and Schweizerhof and Ramm (1984). The last term in Equation (10) contributes to the tangent stiffness matrix, and the discretized equations of motion take the form

$$^1(\mathbf{K}_1 + \mathbf{K}_G - \mathbf{K}_L)\Delta\mathbf{q} = {}^2\mathbf{Q} - \mathbf{M}^2\ddot{\mathbf{q}} - {}^1\mathbf{R}, \tag{11}$$

in which

$$\mathbf{K}_L = \frac{\partial\mathbf{Q}}{\partial\mathbf{q}} \tag{12}$$

is the load stiffness matrix. In nonconservative loading cases the load stiffness matrix is unsymmetric.

BEAMS WITH SOLID CROSS-SECTION

Kinematics of a beam

The deformation of an initially straight beam with undeformable cross-section is studied. With reference to Figure 1, let C be the centroidal axis of the cross-section and $(\hat{\mathbf{e}}_1, \hat{\mathbf{e}}_2, \hat{\mathbf{e}}_3)$ the unit orthonormal vector system in the reference configuration, with $\hat{\mathbf{e}}_1$ along the beam axis (x-axis), and $\hat{\mathbf{e}}_2, \hat{\mathbf{e}}_3$ principal axes of the cross-section (y- and z-axes). A deformed configuration of the beam is then defined by the vector function

$\mathbf{r}(x)$, which characterizes the position of the beam axis, and by the function $\Xi(x)$; an orthogonal matrix defining the rigid rotation of the cross-section at x.

If $\mathbf{x}_o = \mathbf{r}_o + \mathbf{y}_o$ is the material vector in the undeformed reference configuration and $\mathbf{x} = \mathbf{r} + \mathbf{y}$ (vectors $\mathbf{y}$ and $\mathbf{y}_o$ lie on the cross-section plane) the corresponding vector in the deformed state, they are related by the equation

$$\mathbf{x} = \mathbf{r} + \Xi \mathbf{y}_o. \tag{13}$$

The displacement vector $\mathbf{u}$ is then

$$\mathbf{u} = \mathbf{x} - \mathbf{x}_0 = \mathbf{u}_c + (\Xi - \mathbf{I})\mathbf{y}_o, \tag{14}$$

where $\mathbf{u}_c = \mathbf{r} - \mathbf{r}_o$ is the translational displacement vector
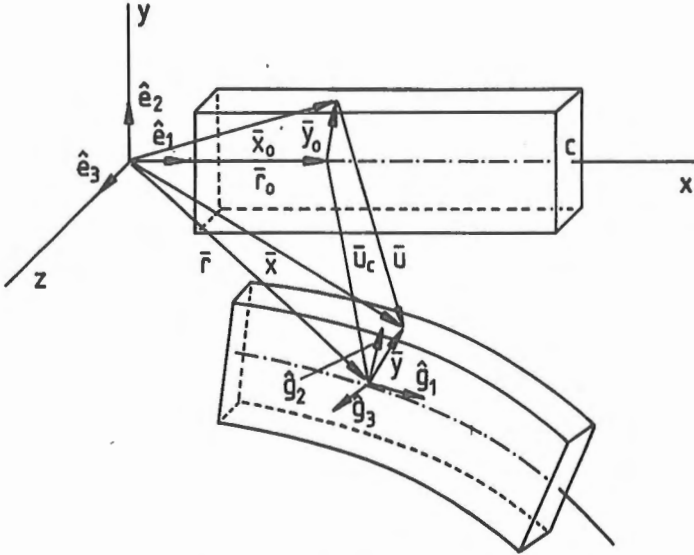
Figure 1. Deformation of a beam.

The rotation matrix can be expressed in concise and elegant form as an exponential of a skew-symmetric matrix

$$\Xi = \exp(\Omega), \qquad \Omega = \begin{bmatrix} 0 & -\theta & \psi \\ \theta & 0 & -\phi \\ -\psi & \phi & 0 \end{bmatrix}, \tag{15}$$

result which may be deduced by arguments based on Lie's theory of groups as is done in quantum mechanics, Argyris (1982). Cartesian components ϕ, ψ, θ define a so-called rotational pseudovector

$$\boldsymbol{\varphi} = [\phi \quad \psi \quad \theta]^T, \qquad \varphi = \|\boldsymbol{\varphi}\| = \sqrt{\phi^2 + \psi^2 + \theta^2}, \tag{16}$$

see Figure 2.

8

Keeping in mind, that the kinematical relations for an updated incremental finite element analysis are sought, assuming small rotation φ, the truncated form of the rotation matrix

$$\Xi = \exp(\mathbf{\Omega}) \approx \mathbf{I} + \mathbf{\Omega} + \tfrac{1}{2}\,\mathbf{\Omega}^2 \tag{17}$$

is used. Rotations ϕ, ψ, θ can then be interpreted as component rotations about cartesian axes x, y, z.
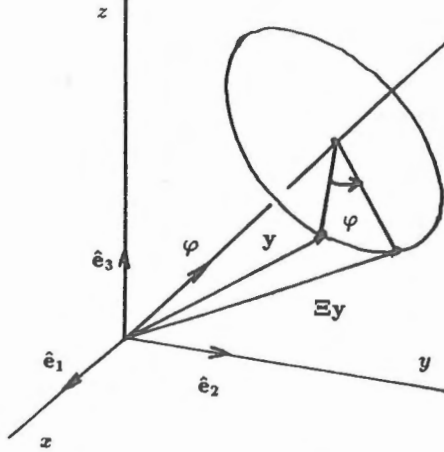
Figure 2. Finite rotation vector φ.

The position vector $\mathbf{y}_o$ and the displacement vectors $\mathbf{u}$ and $\mathbf{u}_c$ are

$$\mathbf{y}_o = \begin{bmatrix} 0 \\ y \\ z \end{bmatrix}, \quad \mathbf{u} = \begin{bmatrix} u \\ v \\ w \end{bmatrix}, \quad \mathbf{u}_c = \begin{bmatrix} u_c \\ v_c \\ w_c \end{bmatrix}, \tag{18}$$

where u_c, v_c and w_c denote the deflections of the centroid axis in the x, y and z ($\hat{\mathbf{e}}_1, \hat{\mathbf{e}}_2, \hat{\mathbf{e}}_3$) directions. Then Equation (14) becomes

$$\begin{aligned}
u &= u_c - (\theta - \tfrac{1}{2}\,\phi\psi)y + (\psi + \tfrac{1}{2}\,\phi\theta)z, \\
v &= v_c - \tfrac{1}{2}\,(\phi^2 + \theta^2)y - (\phi - \tfrac{1}{2}\,\psi\theta)z, \\
w &= w_c + (\phi + \tfrac{1}{2}\,\psi\theta)y - \tfrac{1}{2}\,(\phi^2 + \psi^2)z.
\end{aligned} \tag{19}$$

Equations (19) were obtained by assuming, that the cross-section remains planar during the deformation. However, warping displacements take place when the cross-section is twisted. The warping displacement is assumed to depend on the derivative of the angle of twist, Love (1944), according to equation

$$u_\omega = -\omega(y,z)\phi_{,x}, \tag{20}$$

where ω is the warping function which depends on the cross-section shape, and can be solved from Laplace equation

$$\begin{aligned}
\omega_{,yy} + \omega_{,zz} &= 0 \quad \text{in } A, \\
\text{grad}\,\omega \cdot \hat{\mathbf{n}} &= 0 \quad \text{on } \partial A.
\end{aligned} \tag{21}$$

9

A good approximation to the warping function of a general rectangular cross-section, Bathe and Chaudhary (1982):

$$\omega(y, z) = yz[\omega_1 + \omega_2(z^2 - y^2)]. \tag{22}$$

In the finite element analysis the torque is usually constant within an element. Therefore the expression (22) contains two additional parameters for each element to be solved. These parameters ω_1 and ω_2 can be eliminated by static condensation prior the assemblage of the element matrices into the global structural matrix.

Combining Equations (19) and (20) the kinematical relations for displacement components are

$$
\begin{aligned}
u &= u_c - (\theta - \tfrac{1}{2}\phi\psi)y + (\psi + \tfrac{1}{2}\phi\theta)z - \omega(x,y)\phi_{,x}, \\
v &= v_c - \tfrac{1}{2}(\phi^2 + \theta^2)y - (\phi - \tfrac{1}{2}\psi\theta)z, \\
w &= w_c + (\phi + \tfrac{1}{2}\psi\theta)y - \tfrac{1}{2}(\phi^2 + \psi^2)z.
\end{aligned} \tag{23}
$$

Elements based on Timoshenko beam theory

The only nonvanishing components of the Green-Lagrange strain tensor are

$$
\begin{aligned}
E_x &= u_{,x} + \tfrac{1}{2}(u_{,x}^2 + v_{,x}^2 + w_{,x}^2), \\
E_{xy} &= \tfrac{1}{2}(u_{,y} + v_{,x} + u_{,x}u_{,y} + v_{,x}v_{,y} + w_{,x}w_{,y}), \\
E_{xz} &= \tfrac{1}{2}(u_{,z} + v_{,x} + u_{,x}u_{,z} + v_{,x}v_{,z} + w_{,x}w_{,z}).
\end{aligned} \tag{24}
$$

In the finite element method the displacements $u_c, v_c, w_c, \phi, \psi$ and θ are interpolated by the formulas

$$
\begin{aligned}
u_c &= \mathbf{N}_u \mathbf{q}_u, \\
v_c &= \mathbf{N}_v \mathbf{q}_v, \\
w_c &= \mathbf{N}_w \mathbf{q}_w, \\
\phi &= \mathbf{N}_\phi \mathbf{q}_\phi, \\
\psi &= \mathbf{N}_\psi \mathbf{q}_\psi, \\
\theta &= \mathbf{N}_\theta \mathbf{q}_\theta,
\end{aligned} \tag{25}
$$

where the row matrices $\mathbf{N}_u$ etc. contain the shape functions and the column vectors $\mathbf{q}_u$ etc. the nodal point displacement parameters. By using the kinematical assumptions (23) the expressions for the strain components

$$
\begin{aligned}
\varepsilon_x &= \varepsilon_x(u_c, v_c, w_c, \phi, \psi, \theta), \\
\gamma_{xy} &= \gamma_{xy}(u_c, v_c, w_c, \phi, \psi, \theta), \\
\gamma_{xz} &= \gamma_{xz}(u_c, v_c, w_c, \phi, \psi, \theta)
\end{aligned} \tag{26}
$$

can be derived. The linear strain-displacement matrix $\mathbf{B}$ is obtained from the relationship

$$\delta\varepsilon = \mathbf{B}\delta\mathbf{q} \tag{27}$$

10

between the virtual nodal point displacements and the virtual strains, and it has the form

$$\mathbf{B} = \tag{28}$$

$$\begin{bmatrix} a_1\mathbf{N}_{u,x} & a_2\mathbf{N}_{v,x} & a_3\mathbf{N}_{w,x} & a_4\mathbf{N}_\phi + a_5\mathbf{N}_{\phi,x} & a_6\mathbf{N}_\psi + a_7\mathbf{N}_{\psi,x} & a_8\mathbf{N}_\theta + a_9\mathbf{N}_{\theta,x} \\ b_1\mathbf{N}_{u,x} & b_2\mathbf{N}_{v,x} & b_3\mathbf{N}_{w,x} & b_4\mathbf{N}_\phi + b_5\mathbf{N}_{\phi,x} & b_6\mathbf{N}_\psi + b_7\mathbf{N}_{\psi,x} & b_8\mathbf{N}_\theta + b_9\mathbf{N}_{\theta,x} \\ c_1\mathbf{N}_{u,x} & c_2\mathbf{N}_{v,x} & c_3\mathbf{N}_{w,x} & c_4\mathbf{N}_\phi + c_5\mathbf{N}_{\phi,x} & c_6\mathbf{N}_\psi + c_7\mathbf{N}_{\psi,x} & c_8\mathbf{N}_\theta + c_9\mathbf{N}_{\theta,x} \end{bmatrix},$$

where the abbreviations a_i, b_i and c_i are

$$a_1 = 1 + u_{c,x} - y\theta_{,x} + z\psi_{,x}, \qquad\qquad a_2 = v_{c,x} - z\phi_{,x},$$
$$a_3 = w_{c,x} + y\phi_{,x}, \qquad\qquad a_4 = \tfrac{1}{2}(y\psi_{,x} + z\theta_{,x}),$$
$$a_5 = (y^2 + z^2)|\phi_{,x} - z(v_{c,x} - \tfrac{1}{2}\theta) + y(w_{c,x} + \tfrac{1}{2}\psi),$$
$$a_6 = za_1 + \tfrac{1}{2}y\phi, \qquad\qquad a_7 = -ya_1 + \tfrac{1}{2}z\phi,$$
$$b_1 = -\theta, \qquad\qquad c_1 = \psi,$$
$$b_2 = 1, \qquad\qquad c_2 = -\phi,$$
$$b_3 = \phi, \qquad\qquad c_3 = 1,$$
$$b_4 = w_{c,x} + \tfrac{1}{2}\psi, \qquad\qquad c_4 = -v_{c,x} + \tfrac{1}{2}y\theta_{,x},$$
$$b_5 = -z - \omega_{,y}, \qquad\qquad c_5 = y - \omega_{,z},$$
$$b_6 = \tfrac{1}{2}(\phi + z\theta_{,x}), \qquad\qquad c_6 = 1 + u_{c,x} + \tfrac{1}{2}y\theta_{,x},$$
$$b_7 = -\tfrac{1}{2}z\theta, \qquad\qquad c_7 = \tfrac{1}{2}y\theta,$$
$$b_8 = -1 - u_{c,x} + \tfrac{1}{2}z\psi_{,x}, \qquad\qquad c_8 = \tfrac{1}{2}(\phi + y\psi_{,x}),$$
$$b_9 = \tfrac{1}{2}z\psi, \qquad\qquad c_9 = -\tfrac{1}{2}y\psi$$

Using the strain-displacement matrix $\mathbf{B}$ and the constitutive matrix $\mathbf{C}$, the matrix $\mathbf{K}_1$ in Equation (11) can be written in the form

$$\mathbf{K}_1 = \int_V \mathbf{B}^T\mathbf{C}\mathbf{B}dV, \tag{29}$$

and the internal force vector correspondingly

$$^1\mathbf{R} = \int_V \mathbf{B}^{T1}\tilde{\mathbf{S}}dV, \tag{30}$$

where $^1\tilde{\mathbf{S}}$ is the vector of 2nd Piola Kirchhoff stresses $^1\tilde{\mathbf{S}} = \begin{bmatrix} ^1S_x & ^1S_{xy} & ^1S_{xz} \end{bmatrix}^T$. The geometric stiffness has the form

$$\mathbf{K}_G = \begin{bmatrix} \mathbf{K}_{Guu} & \mathbf{0} & \mathbf{0} & \mathbf{0} & \mathbf{K}_{Gu\psi} & \mathbf{K}_{Gu\theta} \\ & \mathbf{K}_{Gvv} & \mathbf{0} & \mathbf{K}_{Gv\phi} & \mathbf{0} & \mathbf{0} \\ & & \mathbf{K}_{Gww} & \mathbf{K}_{Gw\phi} & \mathbf{0} & \mathbf{0} \\ & & & \mathbf{K}_{G\phi\phi} & \mathbf{K}_{G\phi\psi} & \mathbf{K}_{G\phi\theta} \\ & & & & \mathbf{K}_{G\psi\psi} & \mathbf{K}_{G\psi\theta} \\ \text{s} & \text{y} & \text{m} & \text{m.} & & \mathbf{K}_{G\theta\theta} \end{bmatrix}, \tag{31}$$

in which

$$\mathbf{K}_{Gii} = \int_V {}^1S_x\mathbf{N}_{i,x}^T\mathbf{N}_{i,x}dV, \qquad i = u, v, w,$$

11

$$\mathbf{K}_{G\phi\phi} = \int_V {}^1S_x(y^2 + z^2)\mathbf{N}_{\phi,x}^T\mathbf{N}_{\phi,x}dV,$$

$$\mathbf{K}_{Gw\phi} = \int_V {}^1S_x y\mathbf{N}_{w,x}^T\mathbf{N}_{\phi,x}dV + \int_V {}^1S_{xy}\mathbf{N}_{w,x}^T\mathbf{N}_{\phi}dV,$$

$$\mathbf{K}_{Gv\phi} = -\int_V {}^1S_x z\mathbf{N}_{v,x}^T\mathbf{N}_{\phi,x}dV - \int_V {}^1S_{xz}\mathbf{N}_{v,x}^T\mathbf{N}_{\phi}dV,$$

$$\mathbf{K}_{G\psi\psi} = \int_V {}^1S_x z^2\mathbf{N}_{\psi,x}^T\mathbf{N}_{\psi,x}dV,$$

$$\mathbf{K}_{G\phi\psi} = \tfrac{1}{2}\int_V {}^1S_x y(\mathbf{N}_{\phi_x}^T\mathbf{N}_{\psi} + \mathbf{N}_{\phi}^T\mathbf{N}_{\psi,x})dV + \tfrac{1}{2}\int_V {}^1S_{xy}\mathbf{N}_{\phi}^T\mathbf{N}_{\psi}dV,$$

$$\mathbf{K}_{Gu\psi} = \int_V {}^1S_x z\mathbf{N}_{u,x}^T\mathbf{N}_{\psi,x}dV + \int_V {}^1S_{xz}\mathbf{N}_{u,x}^T\mathbf{N}_{\psi}dV,$$

$$\mathbf{K}_{G\theta\theta} = \int_V {}^1S_x y^2\mathbf{N}_{\theta,x}^T\mathbf{N}_{\theta,x}dV,$$

$$\mathbf{K}_{G\psi\theta} = -\int_V {}^1S_x yz\mathbf{N}_{\psi,x}^T\mathbf{N}_{\theta,x}dV + \tfrac{1}{2}\int_V ({}^1S_{xz}y - {}^1S_{xy}z)\mathbf{N}_{\psi,x}^T\mathbf{N}_{\theta}dV$$
$$+ \tfrac{1}{2}\int_V ({}^1S_{xy}z - {}^1S_{xz}y)\mathbf{N}_{\psi}^T\mathbf{N}_{\theta,x}dV,$$

$$\mathbf{K}_{G\phi\theta} = \tfrac{1}{2}\int_V {}^1S_x z(\mathbf{N}_{\phi_x}^T\mathbf{N}_{\theta} + \mathbf{N}_{\phi}^T\mathbf{N}_{\theta,x})dV + \tfrac{1}{2}\int_V {}^1S_{xz}\mathbf{N}_{\phi}^T\mathbf{N}_{\theta}dV,$$

$$\mathbf{K}_{Gu\theta} = -\int_V {}^1S_x y\mathbf{N}_{u,x}^T\mathbf{N}_{\theta,x}dV - \int_V {}^1S_{xy}\mathbf{N}_{u,x}^T\mathbf{N}_{\theta}dV.$$

The integrations along the x-axis direction have to be done by the one point Gaussian quadrature when linear shape functions for each displacement quantity are used. The one point rule integrates exactly the bending stiffness part and makes the shear stiffness singular, thus the element does not lock when the structure becomes slender. The one point integration yields the same linear stiffness matrix as is obtained by using an additional hierarchical parabolic mode for deflection and condensing out this additional degree of freedom.

Also higher order interpolation can be used yielding an subparametric element. In geometrically nonlinear analysis the interpolation of geometry is important. Much better computational effectivity can be achieved by using a linear isoparametric element.

Over the cross-sectional area either Gauss or Simpson integration rules can be used. In the elastic case and when the cross-section is narrow ($h/b \geq 10$) the 2×2 Gaussian or the 3×3 Simpson's rule is sufficient, although these rules underintegrate the torsional rigidity term

$$I_t = \int_A [(y - \omega_{,z})^2 + (z + \omega_{,y})^2]dA, \tag{32}$$

when the approximate warping function (22) is used. However, the underintegrated torsional rigidity is closer to the exact value than using the 4×4 Gaussian rule, which integrates Expression (32) exactly. When the cross-section is a square the 4×4 Gaussian rule gives the best accuracy, see Table 1.

Table 1. Accuracy of the numerically evaluated torsional rigidity for a rectangular cross-section when approximate warping function (22) is used.

rule		h/b	I_t/hb^3	I_t^{exact}/hb^3	error %	
Gauss	2×2	1	0.091449	0.140577	34.95	
	3×3		0.139012		1.11	
	4×4		0.140741		0.12	$\star$
Simpson	5×5		0.147200		4.71	
	7×7		0.142078		1.07	
Gauss	2×2	4	0.248022	0.280813	11.68	
	3×3		0.275483		1.90	$\star$
	4×4		0.288537		2.75	
Simpson	5×5		0.306217		9.05	
	7×7		0.292496		4.16	
Gauss	2×2	10	0.313838	0.312325	0.48	$\star$
	3×3		0.317249		1.58	
Simpson	5×5		0.330447		5.80	
	7×7		0.324860		4.01	
Gauss	2×2	100	0.333122	0.331233	0.57	$\star$
	3×2		0.333145		0.58	
Simpson	3×3		0.333481		0.68	
	5×3		0.333314		0.63	

$\star$ smallest error

The consistent mass matrix is

$$
\mathbf{M} = \begin{bmatrix}
\mathbf{M}_{uu} & & & & & \\
& \mathbf{M}_{vv} & & & & \\
& & \mathbf{M}_{ww} & & & \\
& & & \mathbf{M}_{\phi\phi} & & \\
& & & & \mathbf{M}_{\psi\psi} & \\
& & & & & \mathbf{M}_{\theta\theta}
\end{bmatrix},
\tag{33}
$$

in which the submatrices $\mathbf{M}_{ii}$ are

$$
\begin{aligned}
\mathbf{M}_{jj} &= \int_V \rho \mathbf{N}_j^T \mathbf{N}_j dV, \qquad j = u, v, w, \\
\mathbf{M}_{\phi\phi} &= \int_V \rho(y^2 + z^2) \mathbf{N}_\phi^T \mathbf{N}_\phi dV, \\
\mathbf{M}_{\psi\psi} &= \int_V \rho z^2 \mathbf{N}_\psi^T \mathbf{N}_\psi dV, \\
\mathbf{M}_{\theta\theta} &= \int_V \rho y^2 \mathbf{N}_\theta^T \mathbf{N}_\theta dV.
\end{aligned}
\tag{34}
$$

For a linear two node element the diagonal mass matrix can be written in the form

$$
\mathbf{M} = \begin{bmatrix}
\mathbf{M}_d & \\
& \mathbf{M}_d
\end{bmatrix},
\tag{35}
$$

13

where the submatrice $\mathbf{M}_d$ has the form

$$\mathbf{M}_d = \frac{m}{2}\begin{bmatrix} 1 & & & & & \\ & 1 & & & & \\ & & 1 & & & \\ & & & I_p/A & & \\ & & & & I_y/A + L^2/12 & \\ & & & & & I_z/A + L^2/12 \end{bmatrix}, \qquad (36)$$

The notations are $I_p = I_y + I_z$, L is the length and $m = \rho A L$ is the mass of an element.

The virtual work expression for internal forces can be formulated using stress resultants and the corresponding generalized strain quantities

$$\int_V {}^2 S_{ij}\delta({}^2 E_{ij})dV = \qquad (37)$$

$$\int_0^L [{}^2N\delta({}^2\varepsilon_c) + {}^2Q_y\delta({}^2\gamma_{xy}) + {}^2Q_z\delta({}^2\gamma_{xz}) + {}^2M_x\delta({}^2\kappa_x) + {}^2M_y\delta({}^2\kappa_y) + {}^2M_z\delta({}^2\kappa_z)]dx,$$

where the stress resultants N, Q_y, Q_z, M_x, M_y and M_z are defined by Equations

$$\begin{aligned} N &= \int_A S_x dA, \\ Q_y &= \int_A S_{xy} dA, \\ Q_z &= \int_A S_{xz} dA, \\ M_x &= \int_A (S_{xz}y - S_{xy}z)dA, \\ M_y &= \int_A S_x z \, dA, \\ M_z &= \int_A S_x y \, dA, \end{aligned} \qquad (38)$$

The generalized strain measures, the elongation ε_c at the cross-section center, the shear strains γ_{xy}, γ_{xz}, the twist per unit length κ_x and the bending curvatures κ_y and κ_z are defined by equations

$$\begin{aligned} \varepsilon_c &= u_{c,x} + \frac{1}{2}[v_{c,x}^2 + w_{c,x}^2 + (I_p/A)\phi_{,x}^2], \\ \gamma_{xy} &= v_{c,x} - \theta + w_{c,x}\phi + \tfrac{1}{2}\phi\psi, \\ \gamma_{xz} &= w_{c,x} + \psi - v_{c,x}\phi + \tfrac{1}{2}\phi\theta, \\ \kappa_x &= \phi_{,x} - \psi\theta_{,x} + \psi_{,x}\theta, \\ \kappa_y &= \psi_{,x} - v_{c,x}\phi_{,x} + \tfrac{1}{2}(\phi\theta_{,x} + \phi_{,x}\theta), \\ \kappa_z &= -\theta_{,x} + w_{c,x}\phi_{,x} + \tfrac{1}{2}(\phi\psi_{,x} + \phi_{,x}\psi). \end{aligned} \qquad (39)$$

In this case the term $u_{,x}^2$ has been neglected in the expression of axial strain.

14

The vectors of stress resultants and generalized strains are denoted by $\mathbf{Q}$ and $\mathbf{e}$, respectively as

$$\mathbf{Q} = \begin{bmatrix} N & Q_y & Q_z & M_x & M_y & M_z \end{bmatrix}^T,$$
$$\mathbf{e} = \begin{bmatrix} \varepsilon_c & \gamma_{xy} & \gamma_{xz} & \kappa_x & \kappa_y & \kappa_z \end{bmatrix}^T. \tag{40}$$

The constitutive law in the elastic case can be written in an incremental form

$$\Delta \mathbf{Q} = \mathbf{C} \Delta \mathbf{e}, \tag{41}$$

with

$$\mathbf{C} = \begin{bmatrix} EA & & & & & \\ & GA_{sy} & & & & \\ & & GA_{sz} & & & \\ & & & GI_t & & \\ & & & & EI_y & \\ & & & & & EI_z \end{bmatrix}, \tag{42}$$

in which EA is the axial rigidity, GA_{sy} and GA_{sz} the shear stiffnesses in y and z directions, GI_t the torsional rigidity and EI_y, EI_z the bending stiffnesses about y and z axes, respectively.

In this case the strain-displacement matrix has the form

$$\mathbf{B} = \tag{43}$$

$$\begin{bmatrix} \mathbf{N}_{u,x} & v_{c,x}\mathbf{N}_{v,x} & w_{c,x}\mathbf{N}_{w,x} & a_1\mathbf{N}_{\phi,x} & \mathbf{0} & \mathbf{0} \\ \mathbf{0} & \mathbf{N}_{v,x} & \phi\mathbf{N}_{w,x} & a_2\mathbf{N}_\phi & a_8\mathbf{N}_\psi & -\mathbf{N}_\theta \\ \mathbf{0} & -\phi\mathbf{N}_{v,x} & \mathbf{N}_{w,x} & a_3\mathbf{N}_\phi & \mathbf{N}_\psi & a_8\mathbf{N}_\theta \\ \mathbf{0} & \mathbf{0} & \mathbf{0} & \mathbf{N}_{\phi,x} & \theta\mathbf{N}_{\psi,x} - \theta_{,x}\mathbf{N}_\psi & \psi_{,x}\mathbf{N}_\theta - \psi\mathbf{N}_{\theta,x} \\ \mathbf{0} & -\phi_{,x}\mathbf{N}_{v,x} & \mathbf{0} & a_4\mathbf{N}_\phi + a_5\mathbf{N}_{\phi,x} & \mathbf{N}_{\psi,x} & a_8\mathbf{N}_{\theta,x} + a_9\mathbf{N}_\theta \\ \mathbf{0} & \mathbf{0} & \phi_{,x}\mathbf{N}_{w,x} & a_6\mathbf{N}_\phi + a_7\mathbf{N}_{\phi,x} & a_9\mathbf{N}_\psi + a_8\mathbf{N}_{\psi,x} & -\mathbf{N}_{\theta,x} \end{bmatrix},$$

where

$$a_1 = I_p\phi_{,x}/A, \qquad\qquad a_2 = w_{c,x} + \tfrac{1}{2}\psi,$$
$$a_3 = \tfrac{1}{2}\theta - v_{c,x}, \qquad\qquad a_4 = \tfrac{1}{2}\theta_{,x},$$
$$a_5 = \tfrac{1}{2}\theta - v_{c,x}, \qquad\qquad a_6 = \tfrac{1}{2}\psi_{,x},$$
$$a_7 = \tfrac{1}{2}\psi + w_{c,x}, \qquad\qquad a_8 = \tfrac{1}{2}\phi,$$
$$a_9 = \tfrac{1}{2}\phi_{,x}.$$

The internal force vector is calculated using the formula

$$^1\mathbf{R} = \int_0^L \mathbf{B}^{T1}\mathbf{Q}\,dx. \tag{44}$$

The geometric stiffness matrix has a little simpler form than in Equation (31)

$$\mathbf{K}_G = \begin{bmatrix} \mathbf{0} & \mathbf{0} & \mathbf{0} & \mathbf{0} & \mathbf{K}_{Gu\psi} & \mathbf{K}_{Gu\theta} \\ & \mathbf{K}_{Gvv} & \mathbf{0} & \mathbf{K}_{Gv\phi} & \mathbf{0} & \mathbf{0} \\ & & \mathbf{K}_{Gww} & \mathbf{K}_{Gw\phi} & \mathbf{0} & \mathbf{0} \\ & & & \mathbf{K}_{G\phi\phi} & \mathbf{K}_{G\phi\psi} & \mathbf{K}_{G\phi\theta} \\ & & & & \mathbf{0} & \mathbf{K}_{G\psi\theta} \\ s & y & m & m. & & \mathbf{0} \end{bmatrix}, \tag{45}$$

15

where the submatrices are †

$$\mathbf{K}_{Gii} = N \int_0^L \mathbf{N}_{i,x}^T \mathbf{N}_{i,x} dx, \qquad i = v, w,$$

$$\mathbf{K}_{G\phi\phi} = NI_p/A \int_0^L \mathbf{N}_{\phi,x}^T \mathbf{N}_{\phi,x} dx,$$

$$\mathbf{K}_{Gw\phi} = M_z \int_0^L \mathbf{N}_{w,x}^T \mathbf{N}_{\phi,x} dx + Q_y \int_0^L \mathbf{N}_{w,x}^T \mathbf{N}_{\phi} dx,$$

$$\mathbf{K}_{Gv\phi} = -M_y \int_0^L \mathbf{N}_{v,x}^T \mathbf{N}_{\phi,x} dx - Q_z \int_0^L \mathbf{N}_{v,x}^T \mathbf{N}_{\phi} dx$$

$$\mathbf{K}_{G\phi\psi} = \tfrac{1}{2} M_z \int_0^L (\mathbf{N}_{\phi,x}^T \mathbf{N}_{\psi} + \mathbf{N}_{\phi}^T \mathbf{N}_{\psi,x}) dx + \tfrac{1}{2} Q_y \int_0^L \mathbf{N}_{\phi}^T \mathbf{N}_{\psi} dx,$$

$$\mathbf{K}_{Gu\psi} = Q_z \int_0^L \mathbf{N}_{u,x}^T \mathbf{N}_{\psi} dx,$$

$$\mathbf{K}_{G\psi\theta} = \tfrac{1}{2} M_x \int_0^L \mathbf{N}_{\psi,x}^T \mathbf{N}_{\theta} dx - \tfrac{1}{2} M_x \int_0^L \mathbf{N}_{\psi}^T \mathbf{N}_{\theta,x} dx,$$

$$\mathbf{K}_{G\phi\theta} = \tfrac{1}{2} M_y \int_0^L (\mathbf{N}_{\phi,x}^T \mathbf{N}_{\theta} + \mathbf{N}_{\phi}^T \mathbf{N}_{\theta,x}) dx + \tfrac{1}{2} Q_z \int_0^L \mathbf{N}_{\phi}^T \mathbf{N}_{\theta} dx,$$

$$\mathbf{K}_{Gu\theta} = -Q_y \int_0^L \mathbf{N}_{u,x}^T \mathbf{N}_{\theta} dx.$$

The internal force vector (44), the geometric stiffness (45) and the linear stiffness matrix

$$\mathbf{K}_1 = \int_0^L \mathbf{B}^T \mathbf{C} \mathbf{B} dx \qquad (46)$$

can now be integrated with respect to the axial coordinate only. This approach results in a simple way to formulate the finite element equations for a three dimensional beam. It is computationally much more economical than a fully numerically integrated element, Equations (29)-(31). However, nonlinear material behaviour cannot be modelled as accurately as in the layered model. For example, in elasto-plastic case the yield surface has to be formulated using the stress resultants, which is quite complicated for general cross-sectional shapes. Therefore simple approximate yield surfaces, expressed in terms of stress resultants, have usually been adopted in the analyses. However, the results of this kind of computations have to be interpreted with great care.

THIN-WALLED BEAMS

Kinematical relations

The kinematic behaviour of beams with thin-walled open cross-section can be derived, based on the assumption that the projection of the cross-section on a plane normal to

---

† In the elastic case $\int_A {}^1 S_x (y^2 + z^2) dA = NI_p/A$. If the material behaves nonlinearly, this approximative expression can still be used, but it may slow down the convergence of the iterative process. In the numerical examples, this retardation has found to be insignificant.

the centroidal axis does not distort during deformation, i.e. the cross-section is rigid in its projection plane. According to this assumption, the in plane displacements of an arbitrary point of the cross-section undergoing a small twisting rotation can be expressed by three parameters: two displacement components v, w and the angle of twist ϕ about the longitudinal beam axis, i.e.

$$
\begin{aligned}
v &= v_c - z\phi, \\
w &= w_c + y\phi.
\end{aligned}
\tag{47}
$$

In this study both elastic and inelastic material behaviour has been investigated, so all displacement quantities are referred to a single point of the cross-section. Transforming v and w in Equation (47) from the x, y, z coordinate system to the orthogonal x, s, r system gives, see Figure 3

$$
\begin{aligned}
\bar{v} &= v \cos \alpha + w \sin \alpha, \\
\bar{w} &= -v \sin \alpha + w \cos \alpha,
\end{aligned}
\tag{48}
$$
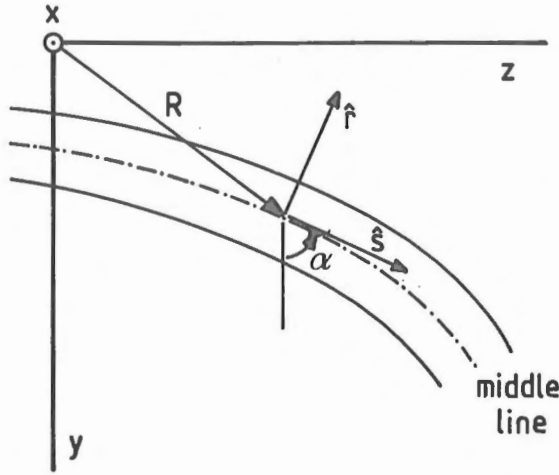
Figure 3. Cross-section of a thin-walled beam.

where $\bar{v}$ and $\bar{w}$ are the displacements of an arbitrary point of the cross-section along the s- and r-axes, respectively, while α denotes the angle between y- and s-axes. Equations (47) and (48) result in

$$
\begin{aligned}
\bar{v} &= v_c \cos \alpha + w_c \sin \alpha + h_s \phi, \\
\bar{w} &= -v_c \sin \alpha + w_c \cos \alpha + h_r \phi,
\end{aligned}
\tag{49}
$$

where

$$
\begin{aligned}
-h_s &= \mathbf{R} \cdot \hat{\mathbf{r}} = z \cos \alpha - y \sin \alpha, \\
h_r &= \mathbf{R} \cdot \hat{\mathbf{s}} = z \sin \alpha + y \cos \alpha.
\end{aligned}
$$

The unit normal vectors $\hat{\mathbf{s}}, \hat{\mathbf{r}}$ and the radius vector $\mathbf{R}$ are, see Figure 3

$$
\begin{aligned}
\hat{\mathbf{s}} &= \cos \alpha \hat{\mathbf{e}}_y + \sin \alpha \hat{\mathbf{e}}_z, \\
\hat{\mathbf{r}} &= -\sin \alpha \hat{\mathbf{e}}_y + \cos \alpha \hat{\mathbf{e}}_z, \\
\mathbf{R} &= y \hat{\mathbf{e}}_y + z \hat{\mathbf{e}}_z,
\end{aligned}
\tag{50}
$$

17

where $\hat{e}_y$ and $\hat{e}_z$ are the unit vectors in the directions of y- and z-axes. Using the linear shear strain expressions

$$\begin{aligned}
\gamma_{xs} &= u_{,s} + \bar{v}_{,x}, \\
\gamma_{xr} &= u_{,r} + \bar{w}_{,x},
\end{aligned} \tag{51}$$

the axial displacement can be integrated from the total differential

$$\begin{aligned}
du &= u_{,s}ds + u_{,r}dr \\
&= (\gamma_{xs} - v_{c,x}\cos\alpha - w_{c,x}\sin\alpha - h_s\phi_{,x})ds \\
&\quad + (\gamma_{xr} + v_{c,x}\sin\alpha - w_{c,x}\cos\alpha - h_r\phi_{,x})dr.
\end{aligned} \tag{52}$$

The shear strain γ_{xs} consists of two parts, i.e. parts due to nonuniform bending γ_{xs}^b and torsion γ_{xs}^t, while the strain γ_{xr} has contribution only due to nonuniform bending:

$$\begin{aligned}
\gamma_{xs} &= \gamma_{xs}^b + \gamma_{xs}^t, \\
\gamma_{xr} &= \gamma_{xr}^b.
\end{aligned} \tag{53}$$

Collecting the terms in Equation (52) in the form

$$\begin{aligned}
du &= \gamma_{xy}^b\cos\alpha\, ds - \gamma_{xy}^b\sin\alpha\, dr - v_{c,x}\cos\alpha\, ds + v_{c,x}\sin\alpha\, dr \\
&\quad + \gamma_{xz}^b\sin\alpha\, ds + \gamma_{xz}^b\cos\alpha\, dr - w_{c,x}\sin\alpha\, ds - w_{c,x}ds \\
&\quad - w_{c,x}\cos\alpha\, dr - (h_s\phi_{,x} - \gamma_{xs}^t)ds - h_r\phi_{,x}dr,
\end{aligned} \tag{54}$$

and using the conventional assumption of the shear strains in the Timoshenko beam theory

$$\begin{aligned}
\gamma_{xy}^b &= v_{c,x} - \theta, \\
\gamma_{xz}^b &= w_{c,x} + \psi,
\end{aligned} \tag{55}$$

with an additional assumption for shear strains due to torsion

$$\gamma_{xs}^t = h_s(\phi_{,x} - \vartheta), \tag{56}$$

where ϑ is an additional displacement variable describing the variation of warping displacement in the longitudinal axis.

Integrating the differential expression in Equation (54) gives the axial displacement

$$u = u_c - y\theta + z\psi - \omega_s\vartheta - \omega_r\phi_{,x}. \tag{57}$$

In the above expression, u_c is an arbitrary function depending only on the x-coordinate, and ω_s is the warping function at the middle line of the cross-section of the member

$$\omega_s(s) = \int_0^s h_s ds. \tag{58}$$

Further, ω_r is the warping function due to the slab action

$$\omega_r(s, r) = h_r(s)r. \tag{59}$$

18

The total torque is a combination of the pure St. Venant's torque M_{xf} and of the warping torque M_ω

$$M_x = M_{xf} + M_\omega,$$
$$M_{xf} = GI_t\phi_{,x},$$
$$M_\omega = GI_s(\phi_{,x} - \vartheta),$$
(60)

where the shear constant I_s is defined by expression

$$I_s = \int_A h_s^2 dA.$$
(61)

The bimoment B is defined by the equation

$$B = -EI_\omega\vartheta_{,x},$$
(62)

where the warping constant I_ω is

$$I_\omega = \int_A \omega_s^2 dA.$$
(63)

The differential equations in terms of the displacement quantities ϕ and ϑ can be obtained from the equilibrium conditions

$$\begin{cases} -(M_\omega + M_{xf})_{,x} = m_x, \\ B_{,x} = M_\omega, \end{cases}$$
(64)

where m_x is the distributed torque along the axis of the bar. Substituting Equations (60) and (63) into the system (64) gives the differential equation system for shear deformable torsion bar

$$\begin{cases} -GI_t\phi_{,xx} - GI_s(\phi_{,xx} - \vartheta_{,x}) = m_x, \\ -EI_\omega\vartheta_{,xx} - GI_s(\phi_{,x} - \vartheta) = 0. \end{cases}$$
(65)

Thin-walled beam element

For a straight beam element with a thin-walled open cross-section, the displacement expressions are almost identical to those used in the case of a beam with a solid cross-section. Only difference is that the warping displacement is divided into two parts,

$$u = u_c - (\theta - \tfrac{1}{2}\phi\psi)y + (\psi + \tfrac{1}{2}\phi\theta)z - \omega_r\phi_{,x} + \omega_s\vartheta,$$
$$v = v_c - \tfrac{1}{2}(\phi^2 + \theta^2)y - (\phi - \tfrac{1}{2}\psi\theta)z,$$
$$w = w_c + (\phi + \tfrac{1}{2}\psi\theta)y - \tfrac{1}{2}(\phi^2 + \psi^2)z.$$
(66)

The twist per unit length is independently interpolated within an element by the shape functions

$$\delta\vartheta = \mathbf{N}_\vartheta\delta\mathbf{q}_\vartheta.$$
(67)

19

In the present case the strain displacement matrix has the form

$$\mathbf{B} = \begin{bmatrix} a_1\mathbf{N}_{u,x} & \cdots & a_4\mathbf{N}_\phi + a_5\mathbf{N}_{\phi,x} & \cdots & a_{10}\mathbf{N}_{\vartheta,x} \\ b_1\mathbf{N}_{u,x} & \cdots & b_4\mathbf{N}_\phi + b_5\mathbf{N}_{\phi,x} & \cdots & b_{10}\mathbf{N}_{\vartheta,x} \\ c_1\mathbf{N}_{u,x} & \cdots & c_4\mathbf{N}_\phi + c_5\mathbf{N}_{\phi,x} & \cdots & c_{10}\mathbf{N}_{\vartheta,x} \end{bmatrix}, \tag{68}$$

where the coefficients are presented in Equation (28) except

$$a_1 = 1 + u_{c,x} - y\theta_{,x} + z\psi_{,x} - \omega_s\vartheta_{,x}, \qquad\qquad a_7 = za_1$$
$$a_9 = -ya_1, \qquad\qquad\qquad\qquad\qquad\qquad a_{10} = \omega_s a_1,$$
$$b_5 = -z - \omega_{r,y}, \qquad\qquad\qquad\qquad\qquad b_{10} = -\omega_{s,y},$$
$$c_5 = y - \omega_{r,z}, \qquad\qquad\qquad\qquad\qquad c_{10} = -\omega_{s,z},$$

Compared to Equation (31) the additional terms in the geometric stiffness matrix are

$$\begin{aligned} \mathbf{K}_{G\vartheta\vartheta} &= \int_V {}^1S_x\omega_s^2\mathbf{N}_{\vartheta,x}^T\mathbf{N}_{\vartheta,x}dV, \\ \mathbf{K}_{G\theta\vartheta} &= \int_V {}^1S_x y\omega_s\mathbf{N}_{\theta,x}^T\mathbf{N}_{\vartheta,x}dV, \\ \mathbf{K}_{G\psi\vartheta} &= -\int_V {}^1S_x z\omega_s\mathbf{N}_{\psi,x}^T\mathbf{N}_{\vartheta,x}dV, \\ \mathbf{K}_{Gu\vartheta} &= -\int_V {}^1S_x\omega_s\mathbf{N}_{u,x}^T\mathbf{N}_{\vartheta,x}dV. \end{aligned} \tag{69}$$

An element stiffness matrix and internal force vector are integrated using the one point Gaussian quadrature in x-axis direction when the linear shape functions are used. Each part of a cross-section has to be integrated at least the 2×2 Gaussian rule. For inelastic analysis higher order rules have to be used.

The consistent mass matrix contains also an additional block, i.e.

$$\mathbf{M}_{\vartheta\vartheta} = \int_V \rho\omega_s^2\mathbf{N}_\vartheta^T\mathbf{N}_\vartheta dV, \tag{70}$$

and the lumped diagonal mass matrix for a two noded element has the same form as in Equation (35), where the seventh diagonal term in the nodal submatrix $\mathbf{M}_d$ is $mI_{\omega_s}/(2A)$.

A thin-walled beam element can also be formulated using the stress resultants and the corresponding generalized strain quantities. The internal virtual work expression for a thin-walled beam is

$$\int_V {}^2S_{ij}\delta({}^2E_{ij})dV =$$

$$\begin{aligned} \int_0^L [{}^2N\delta({}^2\varepsilon_c) + {}^2Q_y\delta({}^2\gamma_{xy}) + {}^2Q_z\delta({}^2\gamma_{xz}) + {}^2M_{xf}\delta({}^2\kappa_x) \\ + {}^2M_y\delta({}^2\kappa_y) + {}^2M_z\delta({}^2\kappa_z) + {}^2B\delta({}^2\kappa_\omega) + {}^2M_\omega\delta({}^2\gamma_\omega)]dx. \end{aligned} \tag{71}$$

The generalized strain measures $\varepsilon_c, \gamma_{xy}, \gamma_{xz}, \kappa_x, \kappa_y$ and κ_z are defined in Equations (39) and in addition

$$\begin{aligned} \kappa_\omega &= -\vartheta_{,x} \\ \gamma_\omega &= \phi_{,x} - \vartheta. \end{aligned} \tag{72}$$

20

Denoting the vector of stress resultants by $\mathbf{Q}$ and the vector of generalized strains by $\mathbf{e}$

$$\mathbf{Q} = \begin{bmatrix} N & Q_y & Q_z & M_{xf} & M_y & M_z & B & M_\omega \end{bmatrix}^T,$$
$$\mathbf{e} = \begin{bmatrix} \varepsilon_c & \gamma_{xy} & \gamma_{xz} & \kappa_x & \kappa_y & \kappa_z & \kappa_\omega & \gamma_\omega \end{bmatrix}^T, \tag{73}$$

the constitutive law in the elastic case can be written in an incremental form

$$\Delta \mathbf{Q} = \mathbf{C} \Delta \mathbf{e},$$

where

$$\mathbf{C} = \begin{bmatrix} EA & & & & & & & \\ & GA_{sy} & & & & & & \\ & & GA_{sz} & & & & & \\ & & & GI_t & & & & \\ & & & & EI_y & EI_{yz} & EI_{y\omega} & \\ & & & & EI_{zy} & EI_z & EI_{z\omega} & \\ & & & & EI_{\omega y} & EI_{\omega z} & EI_\omega & \\ & & & & & & & GI_s \end{bmatrix}. \tag{74}$$

It should be noted that all stress resultants are referred to a single point on the cross-section i.e. on the centroid. In most of the studies of thin-walled beams two reference points, centroid and shear center, are used. However, once some part of the cross-section starts to develop inelastically, the centroid and the shear center as well as the principal axes of the section change continuously with the increasing load. Hence, there seems to be no advantage in adopting such two reference points or making use of the properties of the principal axes.

An element based on Vlasov's classical theory of torsion concerning thin-walled members, Vlasov (1963), can be simply constructed from the presented elements by using a penalty method. In an element, formulated by using the stress-resultants and generalized strain quantities, the Vlasov's constraint

$$\phi_{,x} - \vartheta = 0 \tag{75}$$

can be included in the constitutive matrix $\mathbf{C}$ by substituting term αGI_s instead of GI_s, where α is suitably chosen penalty parameter ($\alpha \gg 1$). To other elements, the constraint (75) can be included by adding a term

$$\alpha GI_s \int_0^L (\phi_{,x}\delta\phi_{,x} - \phi_{,x}\delta\vartheta - \vartheta\delta\phi_{,x} + \vartheta\delta\vartheta)dx \tag{76}$$

in the variational equations.

TRANSFORMATION BETWEEN LOCAL AND GLOBAL COORDINATE SYSTEMS

Orientation of a beam is completely defined in the global X, Y, Z space, if the beam axis and the two directions of the cross-section perpendicular to the beam axis are known.

The orthonormal base vectors in the global coordinate system are denoted by $\hat{\mathbf{G}}_1, \hat{\mathbf{G}}_2$ $\hat{\mathbf{G}}_3$ and the orthonormal base vectors in the beams initial local coordinate system x, y, z by $\hat{\mathbf{g}}_1, \hat{\mathbf{g}}_2, \hat{\mathbf{g}}_3$ in the directions of X, Y, Z and x, y, z axes, respectively, see Figure 4. The initial orientation matrix of a beam can be defined by

$$\mathbf{\Upsilon}_o = \begin{bmatrix} \hat{\mathbf{g}}_1 \cdot \hat{\mathbf{G}}_1 & \hat{\mathbf{g}}_1 \cdot \hat{\mathbf{G}}_2 & \hat{\mathbf{g}}_1 \cdot \hat{\mathbf{G}}_3 \\ \hat{\mathbf{g}}_2 \cdot \hat{\mathbf{G}}_1 & \hat{\mathbf{g}}_2 \cdot \hat{\mathbf{G}}_2 & \hat{\mathbf{g}}_2 \cdot \hat{\mathbf{G}}_3 \\ \hat{\mathbf{g}}_3 \cdot \hat{\mathbf{G}}_1 & \hat{\mathbf{g}}_3 \cdot \hat{\mathbf{G}}_2 & \hat{\mathbf{g}}_3 \cdot \hat{\mathbf{G}}_3 \end{bmatrix}, \tag{77}$$

i.e. the matrix $\mathbf{\Upsilon}_o$ contains the direction cosines

$$\mathbf{\Upsilon}_{oij} = \cos(\hat{\mathbf{g}}_i, \hat{\mathbf{G}}_j) \tag{78}$$

and transfers the global base vectors into the local ones

$$\hat{\mathbf{g}}_i = \mathbf{\Upsilon}_o \hat{\mathbf{G}}_i. \tag{79}$$
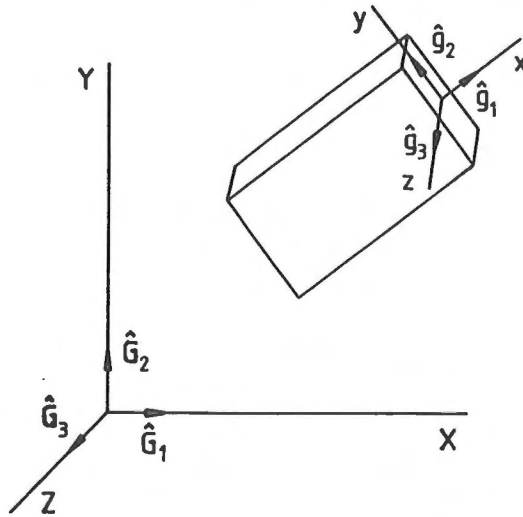
Figure 4. Orientation of a beam.

At some equilibrium configuration C_2', reached after $n+1$ steps, the rotation matrix $\mathbf{R}_{n+1}$ can be obtained from the rotation matrix at previous equilibrium configuration C_1 (at step n) by the formula

$$\mathbf{\Upsilon}_{n+1} = \mathbf{\Delta\Upsilon}\mathbf{\Upsilon}_n, \tag{80}$$

where the incremental rotation matrix $\mathbf{\Delta\Upsilon}$ is calculated from the incremental displacements between steps $n+1$ and n.

In the computer program the initial rotation matrix $\mathbf{\Upsilon}_o$ is formed from the information included in two vectors, the tangent vector of the beam axis $\hat{\mathbf{g}}_1$ and the normal vector of the primary bending plane, or some other given direction of the cross-section plane, $\hat{\mathbf{g}}_3$. Othonormal base of the triple

$$\hat{\mathbf{g}}_1, \hat{\mathbf{g}}_2 = \hat{\mathbf{g}}_1 \times \hat{\mathbf{g}}_3 \quad \text{and} \quad \hat{\mathbf{g}}_3$$

forms the initial rotation matrix Υ_o. If the vector $\hat{g}_3$ is not normal to the principal bending plane, forming an angle φ, the initial rotation matrix is obtained from the orthonormal base $\hat{g}_1, \hat{g}_2, \hat{g}_3$, and the resulting matrix is

$$\Upsilon_o^T = [\,\hat{g}_1 \quad \cos\varphi\hat{g}_2 - \sin\varphi\hat{g}_3 \quad \sin\varphi\hat{g}_2 + \cos\varphi\hat{g}_3\,]. \tag{81}$$

If the element stiffness matrices and the internal force vector are integrated numerically over the cross-sectional area, the transformation (81) is not necessarily needeed.

The element stiffness matrix $\bar{\mathbf{K}}$ and the internal force vector $\bar{\mathbf{R}}$, evaluated in the local coordinate system, are transformed into global coordinate system by formulas

$$\begin{aligned}\mathbf{K} &= \mathbf{T}^T\bar{\mathbf{K}}\mathbf{T}, \\ \mathbf{R} &= \mathbf{T}^T\bar{\mathbf{R}},\end{aligned} \tag{82}$$

where the transformation matrix $\mathbf{T}$ is composed of the rotation matrices

$$\mathbf{T} = \begin{bmatrix} \Upsilon & & \\ & \ddots & \\ & & \Upsilon \end{bmatrix}, \tag{83}$$

where the number of blocks in the diagonal is twice the number of the nodal points in an element. In the case of a thin-walled beam element the transformation matrix has the form, Bažant and El-Nimeiri (1973)

$$\mathbf{T} = \begin{bmatrix} \Upsilon & & & & & & \\ & \Upsilon & & & & & \\ & & 1 & & & & \\ & & & \ddots & & & \\ & & & & \Upsilon & & \\ & & & & & \Upsilon & \\ & & & & & & 1 \end{bmatrix}, \tag{84}$$

where the unit element corresponds to the warping degree of freedom.

CONSTITUTIVE MODELS

Elasto-plastic material model

Incremental constitutive equations which are suitable for computational purposes are usually based on a rate-type plasticity theory by Hill (1959). The strain rate $\mathbf{D}$ is decomposed into elastic and plastic parts

$$\mathbf{D} = \mathbf{D}^e + \mathbf{D}^p. \tag{85}$$

The elastic part $\mathbf{D}^e$ is related to the corotational Zaremba-Jaumann rate of Cauchy stress tensor $\mathbf{T}$ by a linear law

$$\overset{*}{\mathbf{T}} = \mathbf{C}^e : \mathbf{D}^e = \mathbf{C}^e : (\mathbf{D} - \mathbf{D}^p), \tag{86}$$

23

in which $\mathbf{C}^e$ is the elastic constitutive tensor. In the J_2-flow theory, the yield function is

$$f = \sqrt{3J_2} - \sigma(\kappa), \tag{87}$$

where J_2 is the second invariant of the deviatoric Cauchy stress tensor

$$J_2 = -T'_{II} = \frac{1}{2}\mathrm{tr}(\mathbf{T}')^2, \quad \mathbf{T}' = \mathbf{T} - (\frac{1}{3}\mathrm{tr}\mathbf{T})\mathbf{I}, \tag{88}$$

and κ is a hardening parameter. The plastic part of the strain rate is obtained from the plastic potential by the normality law

$$\mathbf{D}^p = \dot{\lambda}\frac{\partial f}{\partial \mathbf{T}} = \dot{\lambda}\mathbf{n}. \tag{89}$$

Using the consistency condition during plastic flow, i.e.

$$\dot{f} = 0 \tag{90}$$

$\dot{\lambda}$ is obtained and Equation (85) gives

$$\overset{*}{\mathbf{T}} = (\mathbf{C}^e - \frac{1}{h}\mathbf{b}\mathbf{b}) : \mathbf{D} = \mathbf{C}^{ep} : \mathbf{D}, \tag{91}$$

where

$$\begin{aligned} \mathbf{b} &= \mathbf{C}^e : \mathbf{n}, \\ h &= \mathbf{n} : \mathbf{C}^e : \mathbf{n} + E_p. \end{aligned} \tag{92}$$

The plastic hardening modulus E_p is obtained from the tangent modulus E_t and the modulus of elasticity E by the formula

$$E_p = \frac{EE_t}{E - E_t}, \quad E_t = \frac{d\sigma_y}{d\bar{\varepsilon}^p}. \tag{93}$$

The yield stress σ_y is obtained from tension tests as a function of the logarithmic inelastic strain

$$\bar{\varepsilon}^p = \int \sqrt{\frac{2}{3}\mathbf{D}^p : \mathbf{D}^p} dt, \tag{94}$$

where t is time or in static analyses a load parameter. In the Lagrangian description a relationship between the 2nd Piola-Kirchhoff stress and the Green-Lagrange strain

$$\dot{\mathbf{S}} = \mathbf{C}_L : \dot{\mathbf{E}} \tag{95}$$

is needed. Taking the time derivative from the expression

$$\mathbf{S} = J\mathbf{F}^{-1} \cdot \mathbf{T} \cdot \mathbf{F}^{-T}, \tag{96}$$

where $J = \rho_o/\rho$ is the determinant of the deformation gradient $\mathbf{F}$, and using the relationship between the strain rate $\mathbf{D}$ and the rate of Green-Lagrange strain

$$\dot{\mathbf{E}} = \mathbf{F}^T \cdot \mathbf{D} \cdot \mathbf{F}, \tag{97}$$

24

yield Equation (95). If small strain assumption is made, the deformation gradient contains only the rigid body rotation, i.e.

$$\mathbf{F} \approx \mathbf{R},$$

and $J = 1$. So, the time derivative of the 2nd Piola-Kirchhoff stress is

$$\dot{\mathbf{S}} = (\mathbf{R}^T \cdot \mathbf{T} \cdot \mathbf{R})^{\cdot} = \mathbf{R}^T \cdot (\dot{\mathbf{T}} - \mathbf{W} \cdot \mathbf{T} - \mathbf{T} \cdot \mathbf{W}^T) \cdot \mathbf{R} = \mathbf{R}^T \cdot \overset{*}{\mathbf{T}} \cdot \mathbf{R}, \qquad (98)$$

where $\mathbf{W}$ is the rate of rotation tensor. Equation (97) has now the form

$$\dot{\mathbf{E}} = \mathbf{R}^T \cdot \mathbf{D} \cdot \mathbf{R}. \qquad (99)$$

Substituting Equation (91) into Equation (98) and taking Equation (99) into account, the relationship between the rate of the 2nd Piola-Kirchhoff stress and the Green-Lagrange strain is obtained

$$\dot{\mathbf{S}} = \mathbf{C}^{ep} : \dot{\mathbf{E}}. \qquad (100)$$

Viscoplastic material model

For rate-dependent material behaviour the strain rate is decomposed into elastic and viscoplastic parts Perzyna (1966) has given the following expression for the viscoplastic part

$$\mathbf{D}^{vp} = \gamma \langle \frac{f}{\sigma_y} - 1 \rangle^p \frac{\partial f}{\partial \mathbf{T}} \qquad (101)$$

where $f = \sqrt{3J_2}$, γ is the viscosity coefficient, σ_y the static yield limit and p is a material parameter. The notation $\langle x \rangle$ has the meaning

$$\langle x \rangle = \begin{cases} 0, & \text{if } x \leq 0; \\ x & \text{if } x > 0. \end{cases} \qquad (102)$$

For isotropic hardening the static yield limit is taken as function of the effective plastic strain $\bar{\varepsilon}^p$

$$\begin{aligned} \sigma_y(\bar{\varepsilon}^p) &= \sigma_{yo} + E_p \bar{\varepsilon}^p, \\ \bar{\varepsilon}^p &= \int_{t_o}^t \sqrt{\frac{2}{3} \mathbf{D}^{vp} : \mathbf{D}^{vp}} dt. \end{aligned} \qquad (103)$$

Thermo-elasto-plastic material

At high temperatures the material parameters, the modulus of elasticity and yield stress decrease. The strain rate is decomposed into elastic, plastic and thermal parts

$$\mathbf{D} = \mathbf{D}^e + \mathbf{D}^p + \mathbf{D}^\theta. \qquad (104)$$

The J_2-flow theory is used to evaluate the plastic strain rate and the thermal strain rate is

$$\mathbf{D}^\theta = \alpha \dot{\theta} \mathbf{I}, \qquad (105)$$

25

where α is the coefficient of thermal expansion which is assumed to be constant. The yield condition is expressed by the formula

$$f = \sqrt{3J_2} - \sigma_y(\kappa, \theta), \tag{106}$$

where the yield stress σ_y depends on a hardening parameter κ and temperature θ. Proceeding as in the previous chapters the corresponding form of the rate equation (100) is obtained.

Yield surfaces expressed in terms of stress resultants

Denoting the vector of stress resultants and the corresponding generalized strains by $\mathbf{Q}$ and $\mathbf{e}$, the yield function can be expressed in the form

$$f(\mathbf{Q}) = 0. \tag{107}$$

For a three dimensional beam with arbitrary cross-sectional shape the function f would be very complex. Yang et al. (1989) have discussed the form of the yield surface for a double symmetric I-sections under five active forces N, M_x, M_y, M_z and B. However, in analysing the response under strong transient loadings, the effect of shear forces becomes important and cannot be neclected from the yield function expression. Simo et al. (1988) have proposed a stress resultant yield function for a plane Timoshenko beam containing the shear force. In this study two simple approximate yield functions have been used. The first one, hypershere has the form

$$\sum_{i=1}^{n_r} (\frac{\mathbf{Q}_i}{\mathbf{Q}_{pi}})^2 = 1, \tag{108}$$

where n_r is the number of stress resultants. The second one, hypercube yield surface is

$$\left| \frac{\mathbf{Q}_i}{\mathbf{Q}_{pi}} \right| = 1, \quad i = 1, ..., n_r. \tag{109}$$

In Equations (108) and (109) $\mathbf{Q}_{pi}$ is the fully plastic value of the corresponding stress resultant. Evaluation of the plastic strains $\Delta\mathbf{e}^p$ and the constitutive matrix C^{ep} is formed similarly to the ones presented in previous chapters.

SOLUTION OF NONLINEAR EQUILIBRIUM EQUATIONS

Discretization of nonlinear equations of a static equilibrium yields a n-dimensional nonlinear algebraic equation system

$$\mathbf{F}(\mathbf{q}, \lambda) \equiv \lambda \mathbf{Q}_r(\mathbf{q}) - \mathbf{R}(\mathbf{q}) = \mathbf{0}, \tag{110}$$

where $\mathbf{q}$ is a n-dimensional vector of displacement quantities, also called a state variable vector, $\mathbf{R}$ the vector of internal resistance forces, $\mathbf{Q}_r$ the reference load vector and λ the load parameter, which now alone characterizes the parametrization of the problem.

Iterative methods have to be used to solve the nonlinear system (110). Usually the $(\mathbf{q}, \lambda)$ path is followed incrementally proceeding from a known equilibrium state $({}^1\mathbf{q}, {}^1\lambda)$ to an adjacent configuration $({}^2\mathbf{q}, {}^2\lambda)$.

In the incremental procedure two strategies have to be chosen: how to proceed from configuration 1 to the next configuration 2 (prediction), and how to improve the predicted solution (correction). The first question is crucial. It has direct influence to the behaviour of the corrector algorithm and so to the cost of computation. Also, depending on the kinematical assumptions made in the formulation of the equilibrium equations, the accuracy of the solution and the reliability of the whole computation process is to a great extent determined by the prediction phase. Thus, the construction of a reliable predictor algorithm is of primary interest.

The arc length Δs between configurations 1 and 2 is defined by equation

$$(\Delta s)^2 = \mathbf{t}^T \mathbf{C} \mathbf{t}, \tag{111}$$

where $\mathbf{t}^T = [\, \boldsymbol{\Delta}\mathbf{q}^T \quad \Delta\lambda \,]$. The prediction step to next configuration can be determined from equations

$$
\begin{aligned}
\boldsymbol{\Delta}\mathbf{q}_Q^1 &= ({}^1\mathbf{K}^{-1}){}^1\mathbf{Q}_r, \\
\Delta\lambda^1 &= \mathrm{sign}({}^1\mathbf{K}) \frac{\Delta s}{\sqrt{(\boldsymbol{\Delta}\mathbf{q}_Q^1)^T \mathbf{W} \boldsymbol{\Delta}\mathbf{q}_Q^1 + \alpha^2}}, \\
\boldsymbol{\Delta}\mathbf{q}^1 &= \Delta\lambda^1 \boldsymbol{\Delta}\mathbf{q}_Q^1,
\end{aligned}
\tag{112}
$$

where the signum operation is defined

$$\mathrm{sign}(\mathbf{K}) = \begin{cases} +1, & \text{if } \mathbf{K} \text{ positive definite;} \\ -1, & \text{otherwise.} \end{cases} \tag{113}$$

A family of corrector algoritms are expressed in the form: solve the iterative changes $\delta\mathbf{q}^i$ and $\delta\lambda^i$ from

$$
\begin{aligned}
\mathbf{K}^{i-1}\delta\mathbf{q}^i &= \delta\lambda^i \mathbf{Q}_r^{i-1} - \mathbf{F}^{i-1}, \\
c(\boldsymbol{\Delta}\mathbf{q}^i, \Delta\lambda^i) &= (\mathbf{t}^i)^T \mathbf{C} \mathbf{n}^i + \theta^i = 0, \\
\delta\mathbf{q}^i &= \delta\lambda^i \delta\mathbf{q}_Q^i + \delta\mathbf{q}_F^i, \\
\delta\mathbf{q}_Q^i &= (\mathbf{K}^{i-1})^{-1}\mathbf{Q}_r^{i-1}, \\
\delta\mathbf{q}_F^i &= (\mathbf{K}^{i-1})^{-1}\mathbf{F}^{i-1}.
\end{aligned}
\tag{114}
$$

In the constraint equation $(114)_2$ a positive definite, or at least positive semidefinite, diagonal weighting matrix is used to make the load parameter and the different displacement quantities commensurable. It is in partitioned form

$$\mathbf{C} = \begin{bmatrix} \mathbf{W} & \\ & \alpha^2 \end{bmatrix}, \tag{115}$$

where the diagonal matrix $\mathbf{W}$ contains the weighting terms of displacements and α is a scaling factor. Matrix $\mathbf{W}$ can also be updated, Tuomala and Kouhia (1986), during

27

the computation in order to adapt the solution algorithm to the particular problem in question. For instance, the emergence of local instabilities could be detected better by the continuation method if the procedure could control more closely those degrees of freedom which change most rapidly.

In this study Fried's orthogonal trajectory method, Fried (1984), is used. It is simple and linear for solving the load parameter change. Vectors $\mathbf{t}, \mathbf{n}$ and scalar θ are

$$\mathbf{t}^i = \begin{bmatrix} \delta \mathbf{q}_Q^i \\ 1 \end{bmatrix}, \qquad \mathbf{n}^i = \begin{bmatrix} \delta \mathbf{q}^i \\ \delta \lambda^i \end{bmatrix}, \qquad \theta^i = 0. \tag{116}$$

With a certain choice of the weighting matrix $\mathbf{W}$, Equations (114) can be identified with single displacement control method, Batoz and Dhatt (1979). If the choice of the controlling displacement is determined independently at each step, the method is similar to Rheinboldt's continuation procedure, Rheinboldt (1986), which also has proved to be reliable and effective, Eriksson (1989). Substituting definitions (116) into Equations (114), the iterative change of load parameter is computed from the equation

$$\delta \lambda^i = -\frac{(\delta \mathbf{q}_Q^i)^T \mathbf{W} \delta \mathbf{q}_F^i}{(\delta \mathbf{q}_Q^i)^T \mathbf{W} \delta \mathbf{q}_Q^i + \alpha^2}. \tag{117}$$

The geometrical interpretation of Fried's orthogonal trajectory method is shown in a one dimensional case in Figure 5. It should be noted that if the tangent stiffness matrix is not updated in the corrective iteration process, Fried's method coincides with the normal plane method, suggested by Ramm (1980) and which is similar to the original method proposed by Riks (1974).
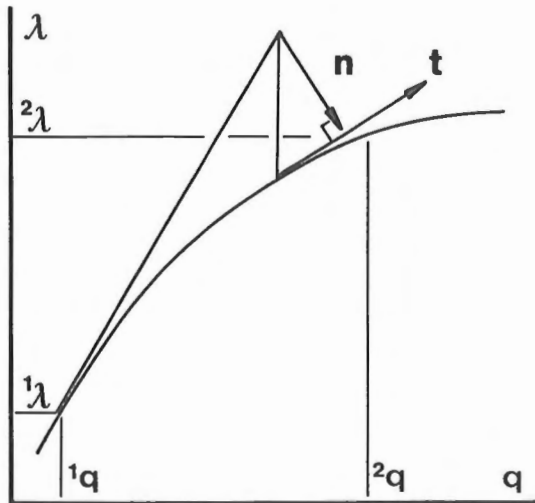
Figure 5. Orthogonal trajectory method.

If a bifurcation point is noticed during the continuation, probably the simplest and most reliable way to branch onto the secondary equilibrium path is to use Fried's

orthogonal trajectory method from the perturbed critical state $\mathbf{q} = \mathbf{q}_{cr} + \Delta s \boldsymbol{\phi}$, $\boldsymbol{\phi}$ is the normalized critical eigenvector. Because this method does not require a known equilibrium point as a starting value, the iteration onto the branch can be started from the perturbed state which is not an equilibrium state.

TIME INTEGRATION METHOD

The semi discrete equations of motion

$$\mathbf{M}^2\ddot{\mathbf{q}} = {}^2\mathbf{Q} - {}^1\mathbf{R} \tag{118}$$

can be solved by a direct time integration method. The explicit central difference method, based on the central difference formulas for the velocity $\dot{\mathbf{q}}$ and for the acceleration $\ddot{\mathbf{q}}$ at time t_n

$$
\begin{aligned}
\dot{\mathbf{q}}_n &= (\mathbf{q}_{n+1} - \mathbf{q}_{n-1})/2\Delta t, \\
\ddot{\mathbf{q}}_n &= (\mathbf{q}_{n+1} - 2\mathbf{q}_n + \mathbf{q}_{n-1})/\Delta t^2,
\end{aligned}
\tag{119}
$$

gives

$$\mathbf{q}_{n+1} = \Delta t^2 \mathbf{M}^{-1}(\mathbf{Q}_n - \mathbf{R}_n) + 2\mathbf{q}_n - \mathbf{q}_{n-1}. \tag{120}$$

In Equation (120) there is an addition of the form $\mathcal{O}(1) + \mathcal{O}(\Delta t^2)$, which gives unfavourable rounding errors when Δt is small, Dahlquist and Björck (1974). It is preferable to use the summed form of the method, where

$$\dot{\mathbf{q}}_{n+\frac{1}{2}} = (\mathbf{q}_{n+1} - \mathbf{q}_n)/\Delta t. \tag{121}$$

Noticing that

$$\dot{\mathbf{q}}_{n+\frac{1}{2}} - \dot{\mathbf{q}}_{n-\frac{1}{2}} = (\mathbf{q}_{n+1} - 2\mathbf{q}_n + \mathbf{q}_{n-1})/\Delta t$$

gives the summed form of the central difference (CD) formulas

$$
\begin{aligned}
\dot{\mathbf{q}}_{n+\frac{1}{2}} &= \dot{\mathbf{q}}_{n-\frac{1}{2}} + \Delta t \ddot{\mathbf{q}}_n, \\
\mathbf{q}_{n+1} &= \mathbf{q}_n + \Delta t \dot{\mathbf{q}}_{n+\frac{1}{2}}, \\
\ddot{\mathbf{q}}_{n+1} &= \mathbf{M}^{-1}(\mathbf{Q}_{n+1} - \mathbf{R}_{n+1}),
\end{aligned}
\tag{122}
$$

in which $t_{n+\frac{1}{2}} = t_n + (\Delta t)/2$.

The central difference method is only conditionally stable, and the time step is limited to

$$\Delta t \leq \Delta t_{cr} = \frac{2}{\omega_{max}}, \tag{123}$$

where ω_{max} is the highest natural frequency of the structure.

NUMERICAL EXAMPLES

A cantilever beam with a solid cross-section (section proportion $h/b = 2$) under a consentrated torque in it's free end is analysed using elastic perfectly plastic material model. The fully plastic torque M_{xp}, predicted by the Nadai's sand heap analogy is

$$M_{xp} = \tau_y W_{xp}, \qquad W_{xp} = \frac{b^2}{6}(3h - b) = \frac{5}{6}b^3.$$

29

The simple expression (22) for the warping of the beam gives fairly good results compared to the analytical, Smith and Sidebottom (1965), and numerical solutions made by a cellular analogy method, Johnson (1988). The computed maximum load was $1.03\ M_{xp}$ after 30 load increments at the point where the angle of twist per unit lenght has the value $\phi' = 2M_{xp}/GI_t$. Calculated load displacement curves are shown in Figure 6.
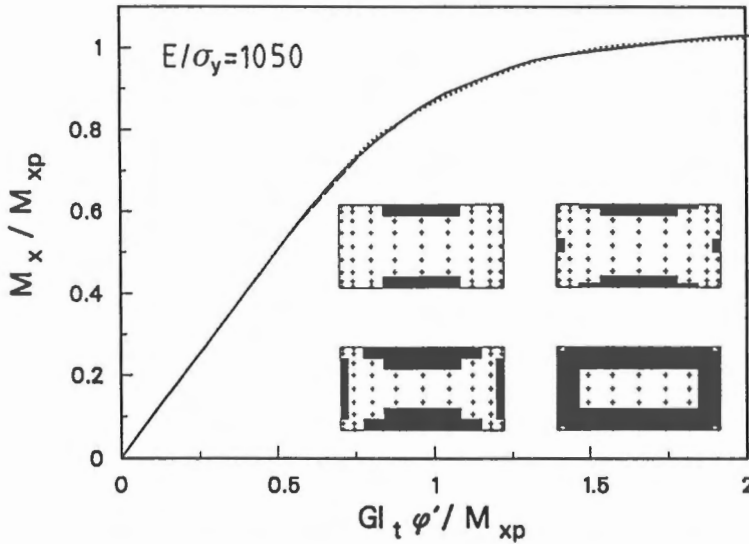
Figure 6. Elasto-plastic torsional response of a beam with a rectangular cross-section. Solid curve indicates computations with the 9×9 Gaussian integration, dotted line the 9×9 Simpson's rule. The plastic areas are shown at load levels $M_x/M_{xp} = 0.7, 0.8, 0.9$ and 0.98.

Elasto-plastic torsional behaviour of a cantilever beam with a thin-walled I-section is also studied. When there are no warping restraints, the torque is carried by the St. Venant shear stresses, and the fully plastic solution is given by the sand heap analogy. For a thin-walled I-beam a close approximation to the fully plastic sand heap torque is

$$M_{xp} = \frac{t_w^2}{6}(3h - t_w) + \frac{t_f^2}{3}(3b - t_f),$$

where t_w and t_f are the web and flange thicknesses, h the depth of a beam between flange centroids and b the breadth of flanges. However, in most structures in which torsion is significant, there are warping restraints at the ends of the members. It is known that the maximum load carrying capacity of a twisted I-beam with warping restraints is higher than the sand heap value, but there is no exact theoretical solution. An upper bound for the total torque M_{xo} at plastic collapse is given by Dinno and Merchant (1965)

$$M_{xo} = M_{xp} + \frac{h}{L}\sigma_y \frac{t_f b^2}{4}.$$

30
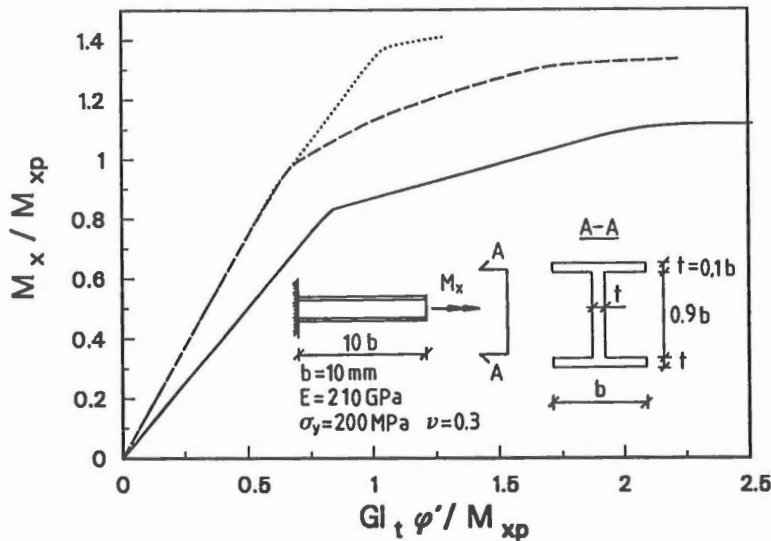
Figure 7. Elasto plastic behaviour of a cantilever I-beam. Solid curve corresponds to the pure St. Venant's torsional behaviour and dashed line indicates the load-deflection curve computed with elements containing warping degrees of freedom. The 4×4 Gaussian integration rule in every cross-section part is used. Dotted line is the result of computation with the 2×2 Gaussian rule at each cross-section part.

The cantilever beam shown in Figure 7 is analysed using a four element mesh where the nodal point coordinates x_j have been graded polynomially according to the grading function

$$\Gamma(x_j) = x_j^{\beta},$$

where $\beta = 3$, see Babuška and Szabo (1983). The cross-section is constructed of five rectangular parts in which the 4×4 Gaussian integration rule is used in each part, separately. The calculated load-deflection curve is shown in Figure 7. The maximum torque obtained in the present calculation was 1.33 M_{xp}, which is slightly greater than Dinno's and Merchant's upper bound value 1.31 M_{xp}. The problem is also analysed using the element which does not contain the warping degrees of freedom. The corresponding load-deflection curve is shown in Figure 7 by solid line and the collapse torque obtained is 1.12 M_{xp} when the 4×4 Gaussian rule is used in each part of the cross-section. The same problem has also been analysed by Bathe and Wiener (1983). They have constructed the web and flanges from nine 4 noded isoparametric beam elements with 6 degrees of freedom at each node and used constraint equations to tie the parts together. The results obtained in the present study are in good agreement with the results obtained by Bathe and Wiener (1983).

Large deflection analysis of a circular bend

The response of a cantilever 45-degree bend subjected to a concentrated end load is

31

calculated. The bend is modelled with eight straight linear elements and the total force, $7.2\,EI/R^2$, is divided into 10, 20 or 60 equal load increments. The pure load controlled Newton method is used to solve the nonlinear equations of equilibrium. The load-tip deflection curves are shown in Figure 8, when 20 equal load increments are used. In the figure also the results from calculation with eight beam-column elements, Virtanen and Mikkola (1985), is presented. They agree well with the present results. Calculated tip deflections are compared to those reported in Bathe and Bolourchi (1979), Simo and Vu-Quoc (1986), Dvorkin et al. (1988), Surana and Sorem (1989) and Sandhu et al. (1990) in Table 2.

Table 2. Comparison of tip deflections of a circular bend.

	NEL	shape f.	$NINC$	$-u/R$	$-v/R$	w/R
present	8	linear	10	0.135	0.231	0.533
present	8	linear	20	0.137	0.230	0.533
present	8	linear	60	0.137	0.229	0.532
Bathe and Bolourchi	8	cubic	60	0.134	0.235	0.534
Simo and Vu-Quoc	8	linear	3	0.135	0.235	0.534
Cardona and Geradin	8	linear	6	0.138	0.237	0.535
Dvorkin et al.	5	parabolic	10	0.136	0.235	0.533
Surana and Sorem	8	parabolic	7	0.133	0.230	0.530
Sandhu et al.	8	linear	3	0.134	0.234	0.533

NEL : number of elements
$NINC$: number of load steps

Tezcan's frame

A high frame, shown in Figure 9 is analysed. The behaviour of the same frame has also been studied by Tezcan and Mahapatra (1969) and Virtanen and Mikkola (1985). The frame is modelled using 72 linear Timoshenko beam elements (eight elements for a column and four for a beam). The values of 206 GPa and 0.25 for Young's modulus and Poisson's ratio are used.

In the present computation a bifurcation point occurred at the load level of 1235 kN, which is not noticed in the other studies. The post buckling behaviour contains the rotational mode about the vertical axis (z-axis) and also small horizontal deflections in the x-axis direction, however, the determination of the post-buckling behaviour did not succeed. Preventing the displacement in y-axis direction and the rotation about z-axis, the equilibrium path shown in Figure 10 is computed. During the load step between the load values of 1348 kN and 1507 kN two eigenvalues became negative.
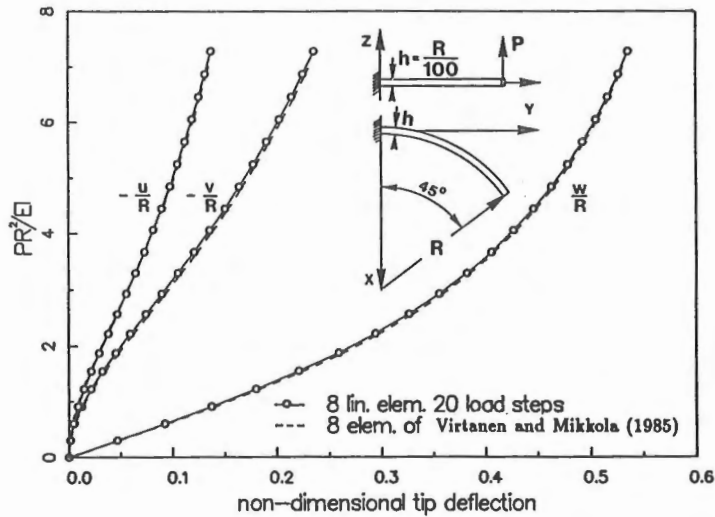
Figure 8. Large deflection analysis of a circular bend.

	columns	beams
$A \ / \ 10^3$ mm^2	22.806	11.006
$I_t \ / \ 10^6$ mm^4	5.4651	1.4027
$I_y \ / \ 10^6$ mm^4	143.64	31.176
$I_z \ / \ 10^6$ mm^4	446.88	94.776
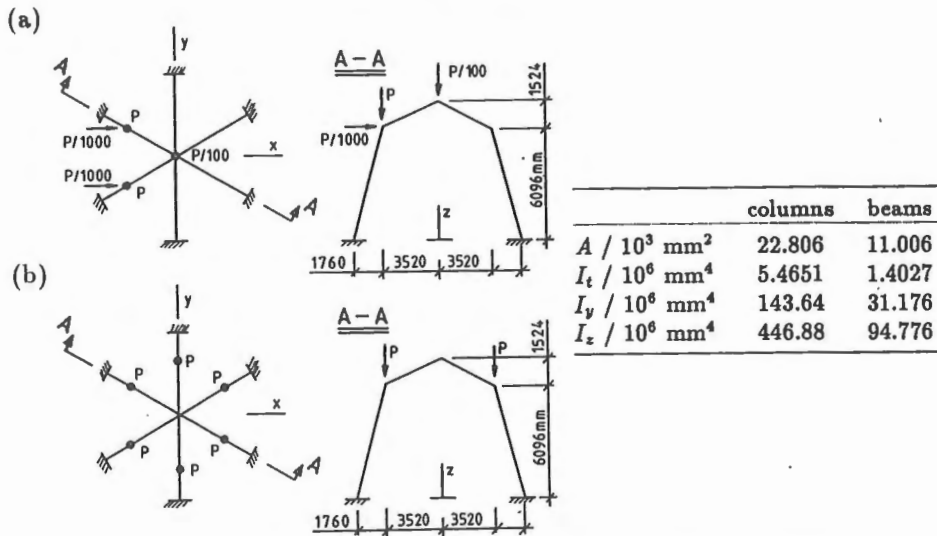
Figure 9. Geometry and loadings of the Tezcan's frame: (a) unsymmetric loading case
analysed in the present study and by Tezcan and Mahapatra (1969) and Virtanen and
Mikkola (1985), (b) symmetric loading case analysed in the present study.

The bifurcation condition is not satisfied and the computation is continued onto the
basic path. Despite of the existence of negative eigenvalues the load-deflection curve
is increasing. The load-deflection curve deviates significantly from the one obtained by
Tezcan and Mahapatra but is qualitatively similar to the result presented by Virtanen
and Mikkola. In those analyses a coarse mesh in which only one element per a member
is used. If the problem is analysed using two elements per a member (Virtanen and

33

Mikkola beam-column element) the result seems to converge to that of present analysis. The deflected shape of the frame at the load level of 1960 kN is shown in Figure 10. It can be seen from the figure that the two colums bearing the vertical loads P buckle.
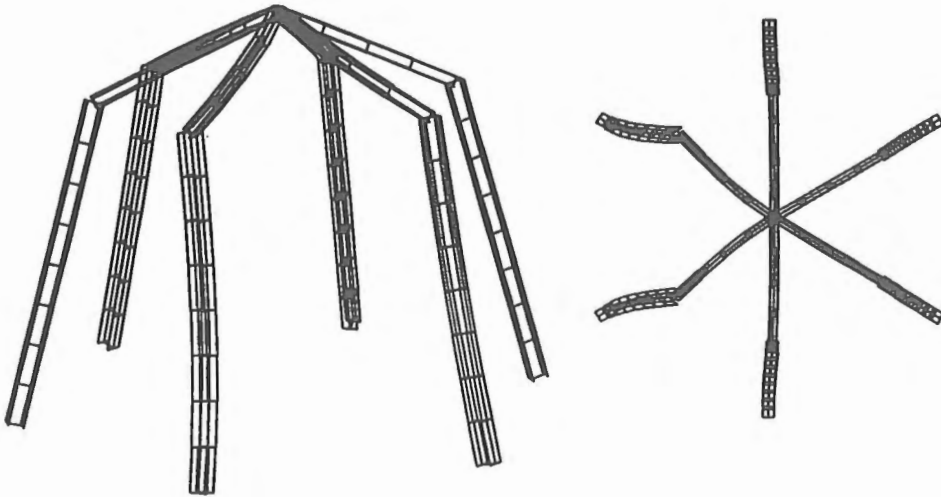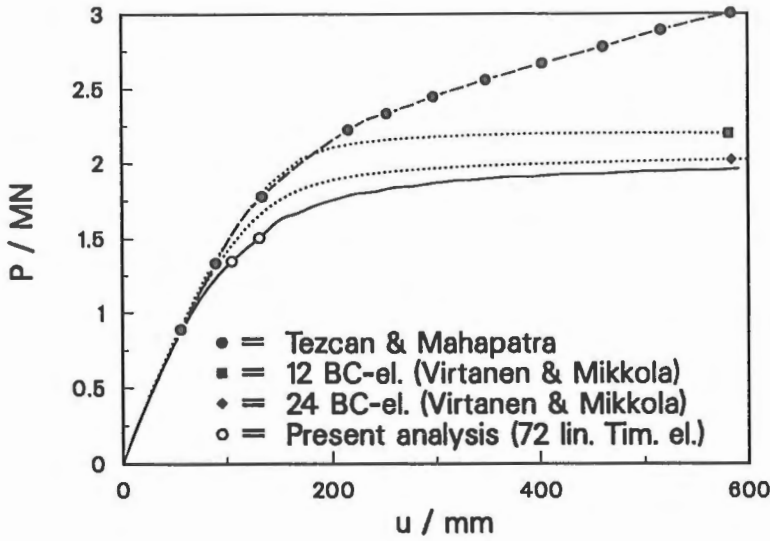
Figure 10. Displacement in x-axis direction at the point C vs. load. The blanked circles indicate the load step in which negative eigenvalues are noticed. Deformed shape at load level $P=1960$ kN.

In the case of symmetric loading, a bifurcation occurred at the load level of 1035 kN, and the post buckling deformation shape was the rotational mode about the vertical axis. In this case there is no difficulty in branching onto the secondary path.

Lateral buckling analysis of cantilever beams

In this section various analyses concerning the behaviour of cantilever beams have been made. First example is a long beam with a narrow solid cross-section ($h/b = 16.129, L/h = 40$). This example has been studied both theoretically and experimentally by Woolcock and Trahair (1974). The lateral displacement-load curves shown in Figure 11 are in close agreement with the results of Woolcock and Trahair. The beam is modelled by ten equal Timoshenko beam elements and the initial load increment used is $\Delta P_0 = 0.5\sqrt{EI_yGI_t}/L^2$. The obtained bifurcation loads are $P_{cr} = 4.085\sqrt{EI_yGI_t}/L^2$ without the effect of the selfweight and $P_{cr} = 3.159\sqrt{EI_yGI_t}/L^2$ including it. As a classical result, without selfweight, the load factor is 4.13, Timoshenko and Gere (1963). The exact critical load including the effect of in plane deformations is 4.036 and when the effect of the selfweight is included it is 3.091, Woolcock and Trahair (1974). †
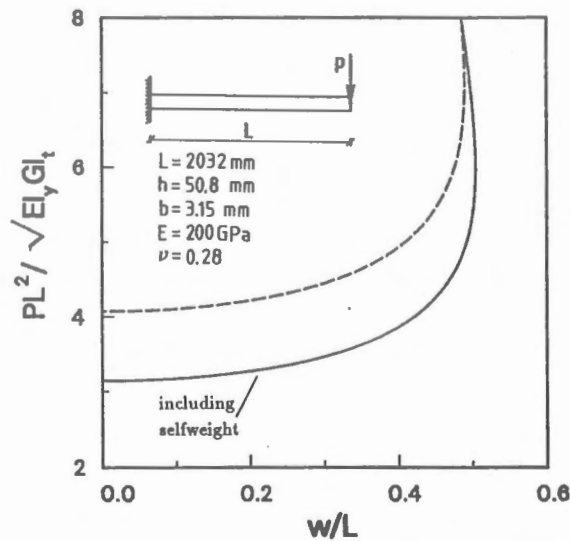
Figure 11. Lateral tip deflections of a narrow rectangular cantilever

Figure 12 shows a load-deflection curve is shown from an analysis of a cantilever beam loaded by a concentrated load at the free end. The load is placed either on the top or on the bottom point of the cross-section. Timoshenko and Gere (1963) give the approximative formula for calculating the critical load

$$P_{cr} = 4.013 \frac{\sqrt{EI_yGI_t}}{L^2}(1 \mp \frac{a}{L}\sqrt{\frac{EI_y}{GI_t}}). \tag{124}$$

---

† There are some discrepancies between the data given in Reference Woolcock and Trahair (1974) at page 160 in Tables 1 and 2. If the value of the expression $\sqrt{EI_yGI_t}/L^2$ is calculated from the information given in the section property table, it will be 1.76229 lbf and if it is calculated from the value given to the classical critical load 7.01 lbf (self weight excluded) in the member detail table, it is 7.01 lbf/4.013 = 1.74682 lbf.

In this formula a denotes the distance of the point of application of the load vertically from the centroid. If the point of application of the load is above the centroid the minus sign is chosen. Table 3 shows the bifurcation loads obtained from an analysis using ten equal Timoshenko beam elements. The length of the beam is L=100 mm, height h=10 mm and width b=1 mm. The in plane tip displacement prior buckling is about 16-17 % of the height of the beam.
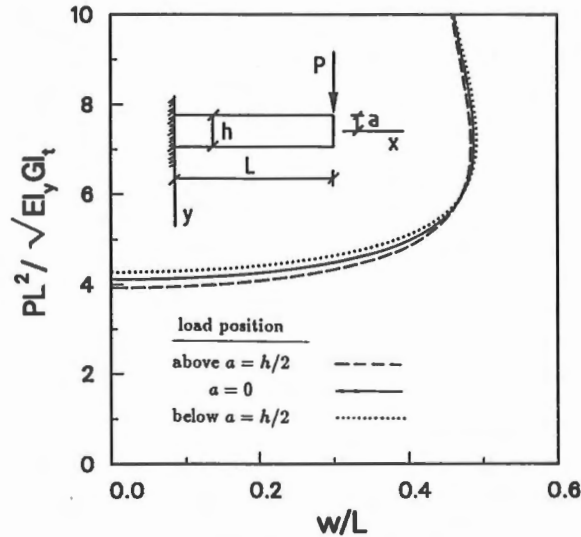
Figure 12. Lateral deflection vs. load of a cantilever beam.

Table 3. Critical load parameter λ_{cr} for a cantilever beam.
$$P_{cr} = \lambda_{cr}\sqrt{EI_yGI_t}/L^2$$

load position	Equation (124)	10 Tim. elem.
above $a = h/2$	3.846	3.913
$a = 0$	4.013	4.124
below $a = h/2$	4.180	4.294

Lateral buckling analysis of a right angle frame

Postbuckling behaviour of a very slender right angle frame is analysed, see Figure 13. Using four elements per a member the buckling load obtained is $P_{cr} = 1.326\sqrt{EI_yGI_t}/L^2$ (1.087 N). The initial load step used is $\Delta P_0 = 0.3\sqrt{EI_yGI_t}/L^2$. The value reported by Argyris et al. (1978) is 1.088 N. In Figure 13 the load-lateral tip deflection curve is shown. If the load direction is reversed (P negative) the buckling occurred at load level of $P_{cr} = -0.838\sqrt{EI_yGI_t}/L^2$. Post buckling path of this computation is also shown in Figure 13.

36
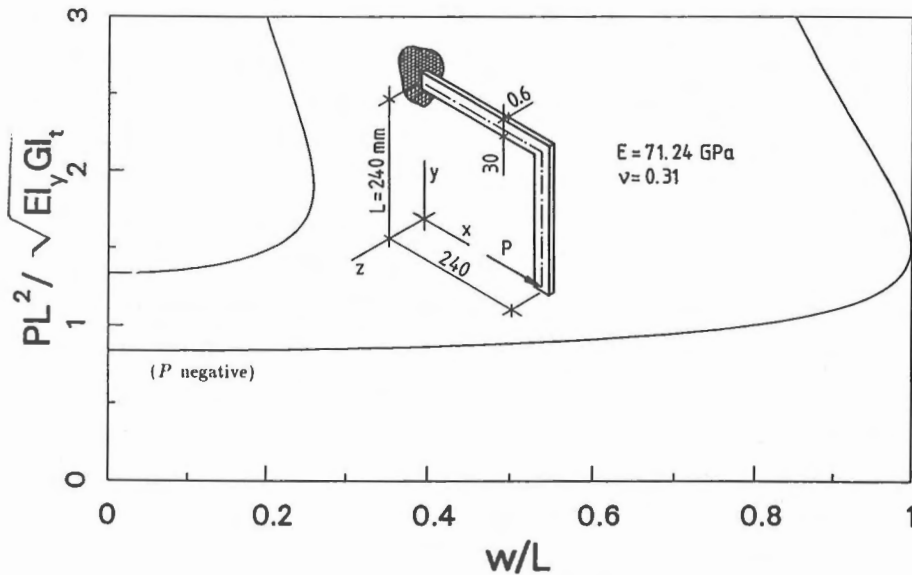
Figure 13. Right angle frame.

This example is particularly tricky if the linear expression $\Xi = \mathbf{I} + \mathbf{\Omega}$ for the rotation matrix is used in formulating the equilibrium equations. In this case wrong buckling loads are obtained i.e. $P_{cr} = 0.668\sqrt{EI_yGI_t}/L^2$ or $P_{cr} = -0.512\sqrt{EI_yGI_t}/L^2$. However, immediately on the post buckling path the load values are increasing toward the value $1.3\sqrt{EI_yGI_t}/L^2$. The convergence of the iterative process is quite slow and the post buckling path seems to be in 5% error to the one shown in Figure 13 and to those reported by Argyris et al. (1979) and Simo and Vu-Quoc (1986).

Elasto-plastic lateral buckling analysis of simply supported I-beams

Kitipornchai and Trahair (1975b) have made an experimental investigation of the inelastic flexural-torsional buckling of rolled steel I-beams. Their tests were carried out on full-scale simply supported 261×151 UB 43 beams with central concentrated loads applied with a gravity load simulator. The 261×151 UB 43 section has a low ratio between the width and thickness of the flanges and so the beam's behaviour inhibits local buckling and allows lateral buckling to predominate. The end cross-sections of each beam were free to rotate about the major and minor axes and to warp. They tested six beams, four as-rolled and two annealed beams. The effect of residual stresses was not found to be significant which was also confirmed by the theoretical predictions made by Kitipornchai and Trahair (1975a) and by numerical computations in the present study. The reason is in high tensile residual stresses which inhibit the spread of plasticity in the compression flange, see Figure 16. The geometrical imperfections were found to be significant in decreasing the load carrying capacity compared to the predictions of the bifurcation loads of perfect structures.

37

Calculated test beams are chosen to be those which buckled in the inelastic range, i.e. beams S2-10, S3-12 and S4-8 (S = simply supported). The imperfection are included in the loading conditions so, that the point load was situated at a small distance from the middle plane of the beam. The cross-section of the beam 261×151 UB 43, the finite element discretizations used and the residual stress patterns are shown in Figure 14. Calculated load-deflection curves are shown in Figure 15.
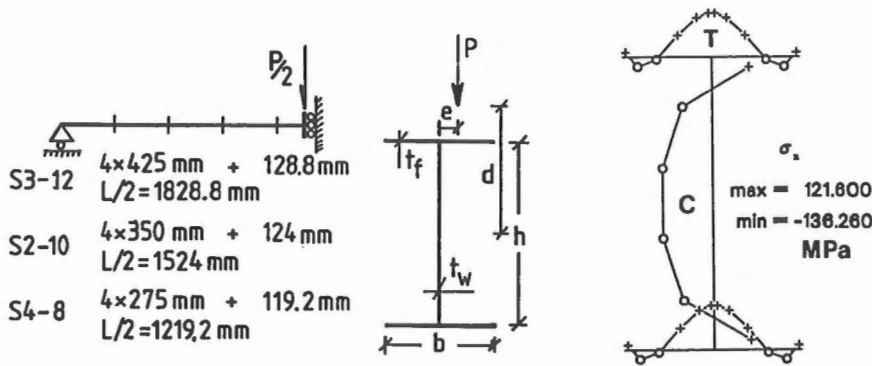
Figure 14. Finite element meshes used and the cross-section 261×151 UB 43 data: $h = 248.7$ mm, $b = 151.5$ mm, $t_w = 7.67$ mm, $t_f = 12.3$ mm and $d = 219$ mm. Residual stress distribution (quartic polynomials) are the same as by Kitipornchai and Trahair (1975b) (Fig. 7, pp. 1340). $E = 203$ GPa, $E_t = E/35$ (except one calculation for S4-8 beam with $E_t = 0$), $\sigma_Y = 320$ MPa, $\nu = 0.3$.

Thermo-elasto-plastic analysis of steel beams

Applications of thermally loaded steel frames are chosen mainly to permit comparisons with the experimental data. Due to the lack of test results of three dimensional cases, only plane frames are analyzed. Two different models for the temperature dependency of material parameters are compared. First model is based on the European recommendations for the fire safety of steel structures (1983). For this model the temperature dependency of Young's modulus E and the yield stress σ_y are shown in Figure 17. Poisson's ratio ν and the tangent modulus E_t are assumed to be independent of temperature. In the second model, similar to the material model of Rubert and Schaumann (1985), a trilinear stress-strain curve is assumed. In that model the variation of Young's modulus, the lower yield stress σ_p and the upper yield stress σ_y are shown in Figure 18.

In all subsequent calculations of the present study a value of $12 \cdot 10^{-6}$ $1/°C$ for the thermal expansion is used. Some calculations for a more accurate description of the thermal expansion coefficient show neglible effect in comparison to the use of its constant value. The thermal expansion has variation from the value of $1.2 \cdot 10^{-5}$ $1/°C$ to $1.7 \cdot 10^{-5}$ $1/°C$ between the range of 20 - 600 °C according to the European recommendations for the fire safety of steel structures.
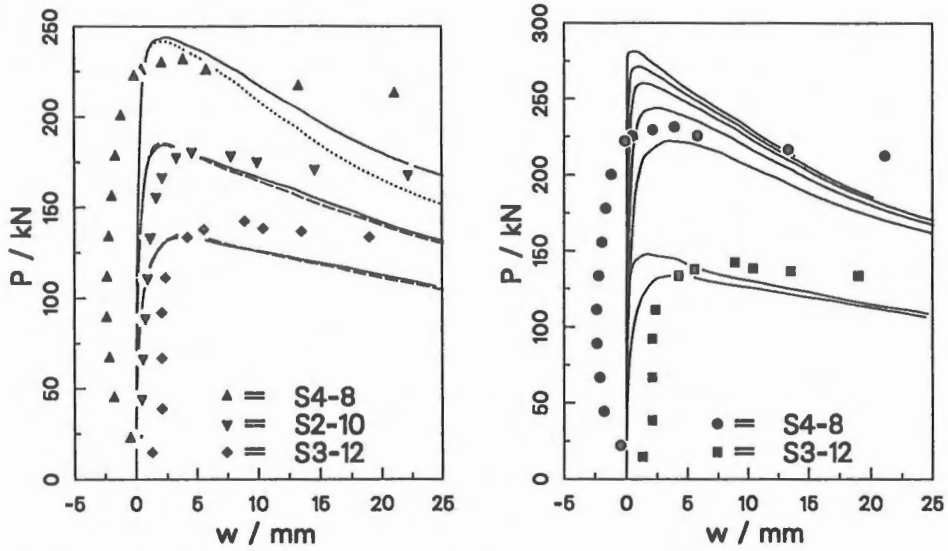
Figure 15. Lateral buckling analysis of simply supported beams. Dashed lines indicate calculations without residual stresses and the dotted line (beam S4-8) is the case with no strain hardening ($E_t = 0$, in all other calculations $E_t = E/35$) Calculations with residual stresses are marked with solid lines. Black markers which are not connected correspond to the experimental measurements. Imperfections in the FE calculations in the figure on the left hand side are: S4-8 $e = 4$ mm, S2-10 and S3-12 $e = 2$ mm; and in the figure on the right hand side: S4-8 $e = 0.25, 1, 2, 4, 8$ mm and S3-12 $e = 0.25, 2$ mm.
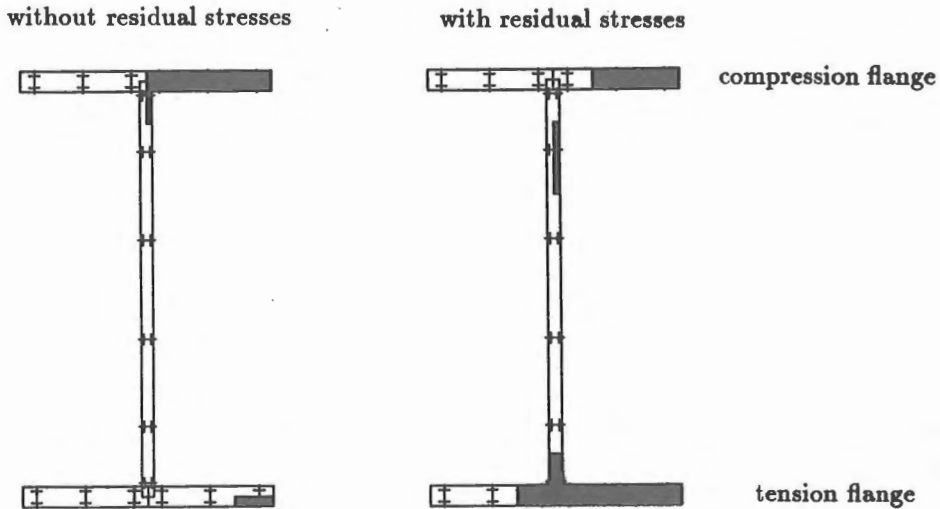
Figure 16. Plastic area of the cross-section at the integration point nearest the symmetry plane, beam S4-8 ($e = 4$ mm) at load level 240 kN.

The only loading effect is due to temperature change. The temperature increment for the following step is adjusted by requiring the estimated norm of the displacement increment to be constant. Denoting

$$u_n = \|\Delta \mathbf{u}_n\|, \qquad v_n = \frac{u_n}{\Delta \theta}, \qquad a_n = \frac{v_n - v_{n-1}}{\Delta \theta},$$

where $\Delta \theta$ is the temperature increment, the requirement for the next step is

$$u_{n+1} = v_n \Delta \theta_{n+1} + \frac{1}{2} a_n (\Delta \theta_{n+1})^2 = u_n,$$

which yields

$$\Delta \theta_{n+1} = \frac{v_n}{a_n} \left(\sqrt{1 + \frac{2 u_n a_n}{v_n^2}} - 1 \right).$$

If $a_n = 0$ the equality $\Delta \theta_{n+1} = \Delta \theta_n$ holds. However, in numerical computations the temperature increment for the next step is determined from the approximate expression

$$\Delta \theta_{n+1} = \frac{u_n}{v_n} \left(1 - \frac{1}{2} \frac{u_n a_n}{v_n^2} \right). \tag{125}$$

Rubert and Schaumann (1985) have made experimental and computational analyses of simply supported IPE-80 beams with a concentrated load at the midspan. Four different load magnitudes are used, $P = 24$ kN, 23 kN, 16kN and 6 kN for beams WK1-4. Corresponding utilization factors are $P/P_u = 0.85, 0.70, 0.50, 0.20$, respectively. Present results of quasi static calculations are compared to the experimental results where the lowest value of the heating rate $\dot{T} = 2.67$ K/min is used. According to the experimental results the effect of heating rate, which were between the values of 2.67 - 32 K/min in the experiments, is not significant to the behaviour of the beams WK1 and WK2. For beam WK4, which has the lowest load, the effect of heating rate results in 10 % difference in the critical temperature. A half of the beam is modelled with five linear elements using two short elements near the symmetry line. Five point and nine point Gaussian quadratures are used in the integration of the stiffness matrix and the internal force vector for flanges and web, respectively. The initial temperature increment used is 20 °C (as in all other examples in this chapter) and it was automatically reduced during the heating process according to Equation (125).

The results of the computations where the material parameters of the second model are used, fits very well to the experimental results in this particular example. Especially, the infuence of the slow decrease interval of the lower yield stress between the temperatures 300-500 °C is clearly seen in the deflection-temperature curves for beams WK1 and WK2, see Figure 20. This slow increase interval of the dispacement has also been noticed in the calculations made by Rubert and Schaumann but it is not visible in the results obtained by Bock and Wernersson (1986) in their calculations using the ADINA program. More examples are presented in Kouhia et al. (1988) and Kouhia (1990).

40
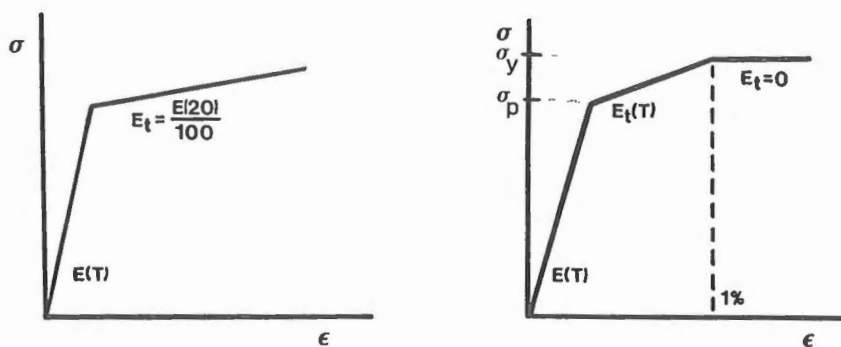
Figure 17. Uniaxial stress-strain relationship which is used in accordance with (a) ECCS model (model 1) and (b) the model developed by Rubert and Schaumann (model 2).
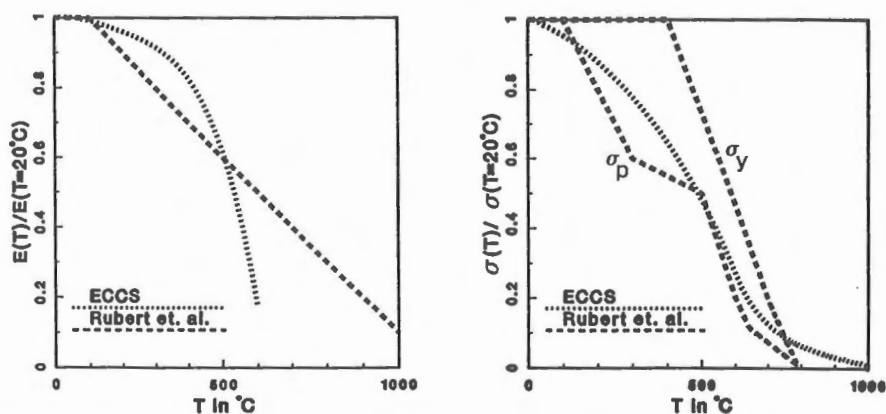
Figure 18. Modulus of elasticity and yield stress as a function of temperature.

Dynamic elasto-plastic behaviour of a portal frame

A portal frame, clamped at its supports, with a mass fixed in the midspan of the horizontal beam, is subjected to an impact load perpendicular to the plane of the frame by a 0.22 lead bullet. Experimental results have been reported by Messmer (1987), and Messmer and Sayir (1988). The loading time have been between the range of 40 to 60 μs, and the measured shape of the load pulse is almost triangle, Figure 4 in Reference Messmer and Sayir (1988). However, the shape and the loading time variations (40-60 μs) have a little influence to the response of the frame. In the present calculations the rectangular pulse, shown in Figure 20 (duration 60 μs and impulse 0.72 Ns), is used. One half of the frame is modelled by using twenty equal elements. In Figure 20 the lateral displacements of the impacted point are shown when the linear Timoshenko beam element is used in the computation. Both elasto-plastic and visco-plastic material models are used in the analyses. When the layered models are used the 7×7 Gaussian

41
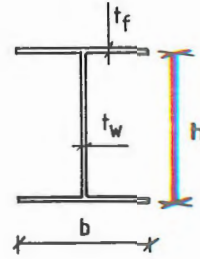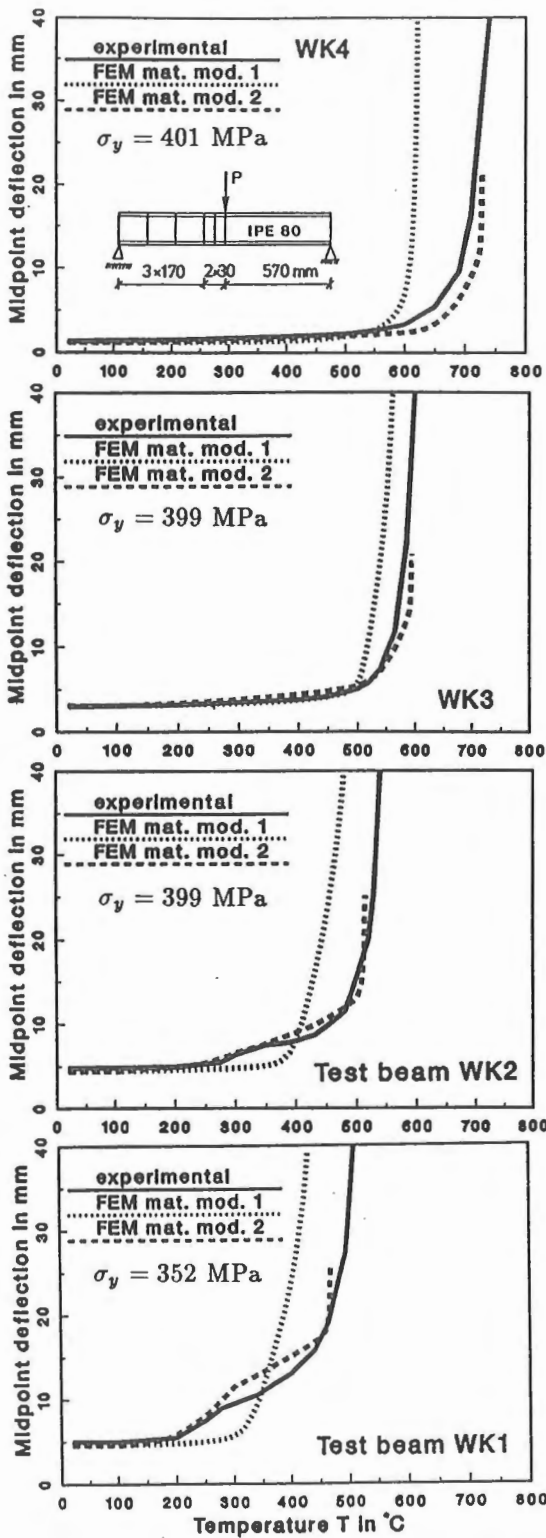
Figure 19. Deflections of the midspan as a function of temperature for a simply supported beam.

quadrature is adopted. Two versions of the Perzyna's viscoplastic material is used. In the first one the viscoplastic part of the strain rate has the form

$$\dot{\varepsilon}_{ij}^{vp} = \sum_{\alpha=1}^{5} B_\alpha \langle \frac{\sigma_e}{\sigma_y} - 1 \rangle^\alpha \frac{\partial f}{\partial \sigma_{ij}}, \tag{126}$$

and in the second one

$$\dot{\varepsilon}_{ij}^{vp} = \gamma \langle \frac{\sigma_e}{\sigma_y} - 1 \rangle^p \frac{\partial f}{\partial \sigma_{ij}}, \tag{127}$$

where the parameters used are $\gamma = 40$ 1/s and $p = 5$. In equations (126) and (127) the notations $f = \sigma_e = \sqrt{3J_2}$ are used. Perzyna has determined the material constants B_α from the experiments made by Clark and Duwez, Perzyna (1966). They are given in Table 4.

Table 4. Material parameters B_α in Equation (126).

α	1	2	3	4	5
B_α (1/s)	337.53	-1470.56	3271.71	-3339.98	1280.06
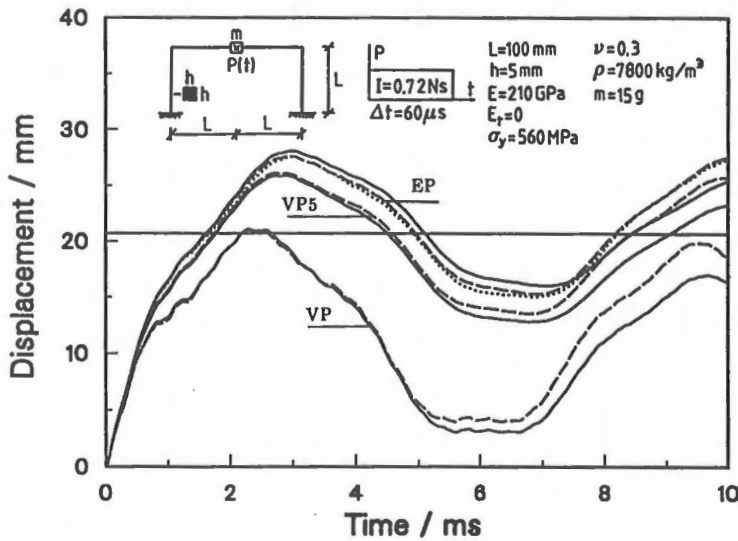
Figure 20. Displacement of the mass. Twenty equal linear Timoshenko beam elements. Solid lines correspond to the layered model computations with the 7×7 Gaussian quadrature. Dashed and dotted lines indicate computations where the sphere or the cube yield surface are used. The permanent experimental deflection was 20.7 mm. Notations; EP: elasto-plastic, VP: visco-plastic model (127), VP5: visco-plastic model (126).

It can be concluded that in this particular model the stress resultant representation of the yield surface gives results which are in good agreement with the computations of layered models. The permanent deflections of the mass point fit quite well to the experimental measurements, Messmer (1987), for the elasto-plastic material models. The viscoplastic model (127) gives considerably too small deflections, but the amplitude of the elastic vibration phase is in a satisfactory agreement with the experimental result (about 21 mm), while in the case of elasto-plastic models the amplitudes are too small (about 12 mm).

In the computation with the yield surface (109) the first plastic hinge appears at the impacted point after the time of 29 μs and it disappears at the time of 120 μs for a while. The bending moment reach again the fully plastic moment at the time 160 μs for duration time of 60 μs. There are also plastic deformations in the horizontal beam between the struck and corner points in distance 50-80 mm from the struck point, see Figure 21. It is also confirmed in the experiments, Messmer (1987). At the time of 420 μs the plastic hinges in bending appear at the clampings for a time period of 90 μs and reappears again at the time of 840 μs. The frame swings out elastically after the time 3.59 ms when the plastic hinges disappears at the clampings. There are also small periods of plastic deformation at the time 5.6 ms and between the period 6.4 to 6.8 ms. The computed bending moment histories, shown in Figure 21, are in agreement with Messmer's theoretical calculations.
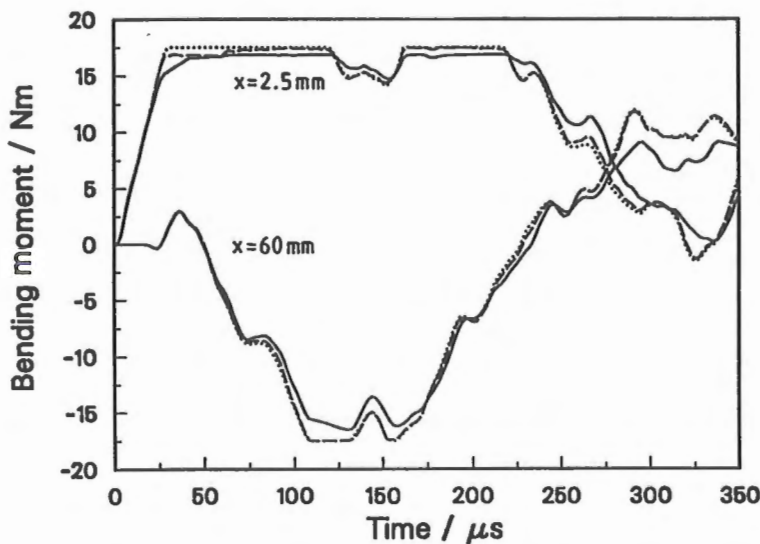
Figure 21. Bending moments in the horizontal beam, (a) 2.5 mm (b) 60 mm from the midspan. The meaning of the different line types are the same as in Figure 20.

44

ACKNOWLEDGEMENTS

REFERENCES

ARGYRIS, J.H., DUNNE, P.C., SCHARPF, D.W., 1978, On large displacement- small strain analysis of structures with rotational degrees of freedom, *Computer Methods in Applied Mechanics and Engineering*, **14**, pp. 401-451.

ARGYRIS, J.H., 1982, An excursion into large rotations, *Computer Methods in Applied Mechanics and Engineering*, **32**, pp. 85-155.

ARGYRIS, J.H., BALMER, H., DOLTSINIS, J.St., DUNNE, P.C., HAASE, M., KLEIBER, M., MALEJANNAKIS, G.A., MLEJNEK, H.-P., MÜLLER, M., SCHARPF, D.W., 1979, Finite element method - the natural approach, *Computer Methods in Applied Mechanics and Engineering*, **17/18**, pp. 1-106.

ARGYRIS, J.H., STRAUB, K., SYMEONIDIS, Sp., 1982, Static and dynamic stability of nonlinear elastic systems under nonconservative forces-natural approach, *Computer Methods in Applied Mechanics and Engineering*, **32**, pp. 59-83.

ATTARD, M.M., 1986, Lateral buckling of the beams by the FEM, *Computers & Structures*, **23** pp. 217-231.

BABUŠKA, I., SZABO, B., 1983, *Lecture Notes on Finite Element Analysis*, manuscript

BARSOUM, R.S., GALLAGHER, R.H., 1970, Finite element analysis of torsional and torsional-flexural stability problems, *International Journal for Numerical Methods in Engineering*, **2** pp. 335-352.

BATHE, K.J., BOLOURCHI, S., 1979, Large displacement analysis of three dimensional beam structures, *International Journal for Numerical Methods in Engineering*, **14** pp. 961-986.

BATHE, K.J., CHAUNDHARY, A., 1982, On the displacement formulation of torsion shafts with rectangular cross-sections, *International Journal for Numerical Methods in Engineering*, **18** pp. 1565-1568.

BATHE, K.J., WIENER, P.M., 1983, On elastic-plastic analysis of I-beams, *Computers & Structures* **17**, pp. 711-718.

BATOZ, J.L., DHATT, G., 1979, Incremental displacement algorithms for nonlinear problems, *International Journal for Numerical Methods in Engineering*, **14**, 1262-1267.

BAŽANT, Z.P., EL NIMEIRI, M., 1973, Large deflection spatial buckling of thin-walled beams and frames, *Journal of Engineering Mechanics*, **99** pp. 1259-1281.

BELYTSCHKO, T., SCHWER, L., KLEIN, M.J., 1977, Large displacement, transient analysis of space frames, *International Journal for Numerical Methods in Engineering*, **11** pp. 65-84.

45

BESSELING, J.F., 1977, Derivatives of deformation parameters for bar elements and their use in buckling and postbuckling analysis, *Computer Methods in Applied Mechanics and Engineering*, **12**, pp. 97-124.

BOCK, H.M., WERNERSSON, H., 1986, Zur rechnerischen Analyse des Tragverhaltens brandbeanspruchter Stahlträger, *Stahlbau*, No 1, pp. 7-14.

CARDONA, A., GERADIN, M., 1988, A beam finite element non-linear theory with finite rotations, *International Journal for Numerical Methods in Engineering*, **26** pp. 2403-2438.

CHEN, H., BLANFORD, G.E., 1989, A C^0 finite element formulation for thin-walled beams, *International Journal for Numerical Methods in Engineering*, **28** pp. 2239-2255.

CHU, K-H., RAMPETSREITER, R.H., 1972, Large deflection buckling of space frames, *Journal of the Structural Division*, ASCE **98**, pp. 2701-2711.

CONNOR, J.Jr., LOGCHER, R.D., CHAN S.C., 1968, Nonlinear analysis of elastic framed structures, *Journal of the Structural Division*, ASCE **94** pp. 1525-1547.

DAHLQUIST, G., BJÖRCK, Å, 1974, *Numerical Methods*, Prentice-Hall, Inc. Englewood Criffs, New Jersey.

DINNO, K.S., MERCHANT, W., 1965, A procedure for calculating the plastic collapse of I-section under bending and torsion, *Structural Engineer*, **43**, pp. 219-221.

DVORKIN, E.N., ONATE, E., OLIVER, J., 1988, On the non-linear formulation for curved Timoshenko beam elements considering large displacement/rotation increments, *International Journal for Numerical Methods in Engineering*, **26** pp. 1597-1613.

EPSTEIN, M., MURRAY, D.,W., 1976, Three dimensional large deformation analysis of thin-walled beams, *International Journal of Solids and Structures*, **12** pp. 867-876.

ERIKSSON, A., 1989, On linear constraints for Newton-Raphson corrections and critical point searches in structural F.E. problems, *International Journal for Numerical Methods in Engineering*, **28**, pp. 1317-1334.

VAN ERP, G.M., 1989, Advanced buckling analyses of beams with arbitrary cross sections. Ph. D. thesis, Technical University of Eindhoven.

VAN ERP, G.M., MENKEN, C.M., VELDPAUS, F.E., 1988, The non-linear flexural-torsional behaviour of straight slender elastic beams with arbitrary cross section, *Thin-Walled Structures*, **6**, pp. 385-404.

European Recommendations for the Fire Safety of Steel Structures, ECCS-Technical Committee 3, Elsevier, 1983.

FRIBERG, P.O., 1985, Beam element matrices derived from Vlasov's theory of open thin-walled elastic beams, *International Journal for Numerical Methods in Engineering*, **21**, pp. 1205-1228.

FRIBERG, O., 1988a, Computation of Euler parameters from multipoint data, *Journal of Mechanisms, Transmission and Automation in Design*, **110**, pp. 116-121.

46

FRIBERG, O., 1988b, A set of parameters for finite rotations and translations, *Computer Methods in Applied Mechanics and Engineering*, **66**, pp. 163-171.

FRIED, I., 1984, Orthogonal trajectory accession to the equilibrium curve, *Computer Methods in Applied Mechanics and Engineering*, **47** pp. 283-297.

HASEGAWA, A., LIYANAGE, K.,K., NISHINO, F., 1987a, A non-iterative nonlinear analysis scheme of frames with thin-walled elastic members, *Structural Engineering / Earthquake Engineering*, **4** pp. 19-29.

HASEGAWA, A., LIYANAGE, K.,K., NODA, M., NISHINO, F., 1987b, An inelastic finite displacement formulation of thin-walled members, *Structural Engineering / Earthquake Engineering*, **4** pp. 269-276.

HIBBIT, H.D., 1979, Some follower forces and load stiffness, *International Journal for Numerical Methods in Engineering*, **14**, pp. 937-941.

HILL, R., 1959, Some basic principles in the mechanics of solids without a natural time, *Journal of Mechanics and Physics of Solids*, **7**, pp. 209-225.

JOHNSON, D., 1988, A cellular analogy for the elastic-plastic Saint-Venant torsion problem, *International Journal of Solids and Structures*, **24**, pp. 321-329.

KITIPORNCHAI, S., TRAHAIR, N.,S., 1975a, Buckling of inelastic I-beams under moment gradient, *Journal of the Structural Division*, ASCE **101** pp. 991-1004.

KITIPORNCHAI, S., TRAHAIR, N.,S., 1975b, Inelastic buckling of simply supported steel I-beams, *Journal of the Structural Division*, ASCE **101** pp. 1333-1347.

KOUHIA, R., PAAVOLA, J., TUOMALA, M., 1988, Modelling the fire behaviour of multistorey buildings, *13th IABSE Congress*, Helsinki, pp. 623-628.

KOUHIA, R., 1990, Nonlinear finite element analysis of space frames, *Helsinki University of Technology, Department of Structural Engineering, Report 109*

KRAHULA, J.L., 1967, Analysis of bent and twisted bars using the finite element method, *AIAA Journal*, **5**, pp. 1194-1197.

KRAJCINOVIC, D., 1969, A consistent discrete elements technique for thinwalled assemblages, *International Journal of Solids and Structures*, **5**, pp. 639-662.

LOVE, A.E.H., 1944, *The Mathematical Theory of Elasticity*, Dover Publ. Inc., New York.

MESSMER, S., 1987, Dynamic elastic-plastic behaviour of a frame including coupled bending and torsion, *Transactions of the 9th International Conference on Structural Mechanics in Reactor Technology*.

MESSMER, S., SAYIR, M., 1988, Dynamic elastic-plastic behaviour of a frame, *Engineering Computation*, **5**, pp. 231-240.

MØLLMANN, H., 1981, Thin-walled elastic beams with finite displacements, *Report R142, Technical University of Denmark, Department of Structural Engineering*.

MOTTERSHEAD, J.E., 1988a, Warping torsion in thin-walled open section beams using the semiloof beam element, *International Journal for Numerical Methods in*

Engineering, **26**, pp. 231-243.

MOTTERSHEAD, J.E., 1988b, Geometric stiffness of thin-walled open section beams using a semiloof beam formulation, *International Journal for Numerical Methods in Engineering*, **26**, pp. 2267-2278.

PAPADRAKAKIS M., 1981, Post-buckling analysis of spatial structures by vector iteration method, *Computers & Structures* **14**, pp. 393-402.

PEDERSEN, C., 1982a, Stability properties and non-linear behaviour of thin-walled elastic beams of open cross-section, Part 1: Basic analysis, *Report R149, Technical University of Denmark, Department of Structural Engineering*.

PEDERSEN, C., 1982b, Stability properties and non-linear behaviour of thin-walled elastic beams of open cross-section, Part 2: Numerical Examples, *Report R150, Technical University of Denmark, Department of Structural Engineering*.

PERZYNA, P., 1966, Fundamental problems in viscoplasticity, *Advances in Applied Mechanics*, **9**, pp. 243-377.

RAJASEKARAN, S., MURRAY, D.W., 1973, Finite element solution of inelastic beam equations, *Journal of Engineering Mechanics*, **99** pp. 1025-1041.

RAMM, E., 1980, Strategies for tracing the nonlinear responce near limit points, in K.J. Bathe et al. (eds.), *Europe-U.S. Workshop on Nonlinear Finite Element Analysis of Structural Mechanics*, Ruhr Universität Bochum, Germany, Springer-Werlag, Berlin, pp. 63-89.

REMSETH, S.N., 1979, Nonlinear static and dynamic analysis of framed structures, *Computers & Structures*, **10**, pp. 879-897.

RENTON, J.D., 1962, Stability of space frames by computer analysis, *Journal of Structural Division*, **88** ST4, pp. 81-103.

RHEINBOLDT, W.C., 1986, *Numerical Analysis of Parametrized Nonlinear Equations*, Wiley, New York.

RIKS, E., 1974, The incremental solution of some basic problems of elastic stability, *Report NLR TR 74005 U*, National Aerospace Laboratory NLR, The Netherlands.

RUBERT, A., SCHAUMANN, P., 1985, Tragverhalten stählerner Rahmensysteme bei Brandbeanspruchung, *Stahlbau*, **54**, pp. 280-287.

SANDHU, J.S., STEVENS, K.A., DAVIES, G.A.O., 1990, A 3-D, co-rotational, curved and twisted beam element, *Computers & Structures*, **35**, pp. 69-79.

SCHWEIZERHOF, K., RAMM, E., 1984, Displacement dependent pressure loads in nonlinear finite element analysis, *Computers & Structures*, **18**, pp. 1099-1114.

SIMO, J.C., 1985, A finite strain beam formulation. The three dimensional dynamic problem, Part I, *Computer Methods in Applied Mechanics and Engineering*, **49** pp. 55-70.

SIMO, J.C., VU-QUOC, L., 1986, A three dimensional finite strain rod model, Part II: Computational aspects, *Computer Methods in Applied Mechanics and Engineering*, **58**

pp. 79-115.

SIMO, J.C., KENNEDY, J.G., GOVINDJEE, S., 1988, Non-smooth multisurface plasticity and viscoplasticity. Loading/unloading conditions and numerical algorithms, *International Journal for Numerical Methods in Engineering*, **26**, pp. 2161-2185.

SEKULOVIĆ, M., 1986, Geometrically nonlinear analysis of thin-walled members, Proceedings *'Steel Structures: Recent Research Advances and Their Applications to Design'*, Elsevier Applied Science Publishers Ltd. pp. 219-243.

SMITH, J.O., SIDEBOTTOM, O.M., 1965, Inelastic Behaviour of Load-Carrying Members, Wiley, New York.

SURANA, K.S., SOREM, R.,M., 1989, Geometrically non-linear formulation for three dimensional curved beam elements with large rotations, *International Journal for Numerical Methods in Engineering*, **28**, pp. 43-73.

TEZCAN, S.S., MAHAPATRA, B.C., 1969, Tangent stiffness matrix for space frame members, *Journal of the Structural Division*, ASCE, **95**, pp. 1257-1270.

TIMOSHENKO, S.P., GERE, J.M., 1961, *Theory of Elastic Stability*, McGraw-Hill, New York.

TUOMALA, M, KOUHIA, R, 1986, Adaptive finite element analysis of geometrically nonlinear elasto-plastic structures, *Report 10, Tampere University of Technology, Department of Civil Engineering, Structural Mechanics.*

VIRTANEN, H., MIKKOLA, M., 1985, Geometrically nonlinear analysis of space frames (in Finnish), *Journal of Structural Mechanics (Rakenteiden Mekaniikka)*, **18**, No 3 pp. 82-97.

VLASOV, V.Z., 1963, *Thin-Walled elastic beams*, Israel Program for Scientific Translations.

WOOLCOCK, S.T., TRAHAIR, N.S., 1974, Post-buckling behaviour of determinate beams, *Journal of the Engineering Mechanics Division*, **100**, pp. 151-171.

WUNDERLICH, W., OBRECHT, H., SCHRÖDTER, V., 1986, Nonlinear analysis and elastic-plastic load-carrying behaviour of thin-walled spatial beams with warping constraints, *International Journal for Numerical Methods in Engineering*. **22** pp. 671-695.

YANG, Y-B., CHERN, S-M., FAN, H-T., 1989, Yield surfaces for I-sections with bimoments, *Journal of Structural Engineering*, **115**, pp. 3044-3058.

ZIEGLER, H., 1968, *Principles of Structural Stability*, Blaisdell Publishing Company.

Reijo Kouhia, senior assistant, Helsinki University of Technology, Laboratory of Structural Mechanics